The Astrophysical Journal, 703:479–499, 2009 September 20 doi:10.1088/0004-637X/703/1/479

DEUTERIUM CHEMISTRY IN PROTOPLANETARY DISKS. II. THE INNER 30 AU

K. Willacy[1] and P. M. Woods[2]
[1] Jet Propulsion Laboratory, California Institute of Technology, MS 169-506, Pasadena, CA 91109, USA; Karen.Willacy@jpl.nasa.gov
[2] Jodrell Bank Centre for Astrophysics, The Alan Turing Building, School of Physics and Astronomy, The University of Manchester, Oxford Road, Manchester, M13 9PL, UK; Paul.Woods@manchester.ac.uk
Received 2009 March 12; accepted 2009 August 7; published 2009 August 27

ABSTRACT

We present the results of models of the chemistry, including deuterium, in the inner regions of protostellar disks. We find good agreement with recent gas-phase observations of several (non-deuterated) species. We also compare our results with observations of comets and find that in the absence of other processing, e.g., in the accretion shock at the surface of the disk, or by mixing in the disk, the calculated D/H ratios in ices are higher than measured and reflect the D/H ratio set in the molecular cloud phase. Our models give quite different abundances and molecular distributions to other inner disk models because of the differences in physical conditions in the model disk. This emphasizes how changes in the assumptions about the density and temperature distribution can radically affect the results of chemical models.

Key words: astrochemistry – circumstellar matter – ISM: abundances – ISM: molecules – solar system: formation – stars: formation – stars: pre-main sequence

Online-only material: color figures

1. INTRODUCTION

Observations and models of the deuterium chemistry in protostellar disks can make important contributions to our understanding of the chemistry of the early solar system. They can be directly related to the chemistry of the formation of cometary ices, which provides a link between the current and primitive solar nebula. Observations of deuterated molecules can be used to trace the physical and thermal history of a protostellar disk and, combined with models, can determine the relative contribution of the different phases of star formation (e.g., molecular cloud, collapse, protostellar disk) to the molecular deuteration ratios observed in protostellar disks and in comets. Although the elemental abundance of deuterium in the Galaxy is only a few $\times 10^{-5}$ (Linsky et al. 2006) the relative abundance of deuterated to non-deuterated molecules can be much higher and depends sensitively on the temperature at which the molecules formed, and, at high densities, on the degree of molecular depletion. Models of the deuterium chemistry have demonstrated the importance of gas-phase reactions of deuterated isotopologues of H_3^+, CH_3^+, and $C_2H_2^+$ in transferring deuterium atoms to molecules, as well as the critical role played by grain surface chemistry, where reactions of deuterium atoms are able to efficiently form molecules such as deuterated formaldehyde and methanol.

A few deuterated molecules have now been observed in protostellar disks. Ceccarelli et al. (2004) observed H_2D^+ in TW Hya and DM Tau, and argued that the emission originates in the midplane and that therefore H_2D^+ provides a means of tracing the ionization level in this high-density, low-temperature region where few other molecules exist in the gas phase. A later paper (Ceccarelli et al. 2005) reported a detection of HDO in DM Tau where the emission is from a region with a temperature of ~ 25 K, far below that at which this molecule can be thermally desorbed. This indicates that there is an efficient non-thermal desorption mechanism acting, e.g., photodesorption (Dominik et al. 2005; Willacy & Langer 2000). (Note that the observations of both H_2D^+ and HDO have been disputed by Guilloteau et al. (2006).) DCO^+ has been observed in TW Hya (Qi et al. 2008; van Dishoeck et al. 2003) and in DM Tau (Guilloteau et al. 2006). van Dishoeck et al. (2003) used JCMT and found a beam-averaged ratio of $DCO^+/HCO^+ = 0.035$. Qi et al. (2008) using the Submillimeter Array (SMA) found a more complex distribution of DCO^+ which does not follow that of HCO^+. In this case, DCO^+/HCO^+ increases with radius between 30 and 70 AU from 0.01 to 0.1, and DCO^+ disappears rapidly at $R > 90$ AU. In contrast, HCO^+ and CO are present out to 200 AU. In DM Tau, Guilloteau et al. (2006) find $DCO^+/HCO^+ \sim 4 \times 10^{-3}$ in the outer disk. Qi et al. (2008) also observe DCN in TW Hya and determine DCN/HCN to be 0.017.

These observations are all for the outer regions of the disk ($R \gtrsim 30$–50 AU). Here our focus is on $R \leqslant 30$ AU. The inner regions of disks are of great interest because they cover the region where planet formation took place in the solar nebula. They are now becoming accessible to observational investigation, e.g., with the *Spitzer Space Telescope* (Carr & Najita 2008; Salyk et al. 2008; Lahuis et al. 2006) or the Keck Interferometer (Gibb et al. 2007, 2004). In the future, Atacama Large Millimeter Array (ALMA) will further open up this region for study.

Solar system data provide an additional constraint on the models. Observations of deuterated molecules in comets are limited to two molecules (HDO and DCN) in four comets—Halley, Hale-Bopp, Hyakutake, and C/2002 T7 LINEAR. The ratios are similar in all of the observed comets with $HDO/H_2O \sim 5$–7×10^{-4} (Bockelee-Morvan et al. 1998; Eberhardt et al. 1995; Balsiger et al. 1995; Hutsemékers et al. 2008) and DCN/HCN $\sim 2 \times 10^{-3}$ (Meier et al. 1998). These values are higher than the solar elemental D/H ratio. The similarities between molecular D/H ratios observed in the interstellar medium and those seen in comets have led to the suggestion that cometary ices have their origin in the interstellar medium. However, there is sufficient difference between the two data sets for this to still be an open question, e.g., Bergin et al. (2007) and to suggest that processing during star formation or in the early solar nebula could affect the ratios. Once comets formed, they are thought to have undergone relatively little subsequent processing and therefore their abundances reflect the composition of material at the time of their formation.

Enhanced D/H ratios are seen elsewhere in the solar system. For example, interplanetary dust particles are enriched in D with respect to the terrestrial value (e.g., Messenger et al. 2003; Messenger 2000). They show an extremely wide range of D/H ratios (Robert et al. 2000) but the carriers have not yet been identified. Enhancements are also seen in primitive meteorites (LL3 and carbonaceous chondrites, as well as meteoritic water), but the anomalies are generally smaller. The observations do not yet allow for the origin of the deuterated material to be definitively identified, and both interstellar (e.g., Pizzarello & Huang 2005) and protostellar (e.g., Remusat et al. 2006) origins have been claimed.

The deuterium content of the giant planets Jupiter and Saturn is considered to be a relic of the early protosolar nebula, since deuterium is neither formed nor destroyed in these planets, and their gravity is sufficient to prevent hydrogen and deuterium from escaping (Owen et al. 1986). Accordingly, measuring their molecular D/H ratios can provide information about the deuteration levels in the protosolar nebula at their time of formation. Measurements in Jupiter suggest that the D/H ratio is enhanced over the interstellar value elemental ratio by a factor of a few. Mahaffy et al. (1998) used the Galileo Probe Mass Spectrometer to derive $(D/H)_{H_2} = 2.6 \pm 0.7 \times 10^{-5}$, in close agreement with the ISO-LWS value of 2.2×10^{-5} (Lellouch et al. 2001). Both these values depend on the models used to analyze the data. A direct measurement of D/H in the limb of Jupiter using Lyα emission was made by Ben Jaffel et al. (1998) who found $(D/H)_{H_2} = 5.9 \times 10^{-5}$. Deuterated methane has also been observed with a ratio $(D/H)_{CH_4} = 1.8 \times 10^{-5}$–$2.9 \times 10^{-5}$ (Feuchtgruber et al. 1999; Encrenaz et al. 1999). Saturn has similar D/H ratios to Jupiter (1.7×10^{-5}; Lellouch et al. (2001)). In Neptune and Uranus, the ratios are higher – 6.5×10^{-5} (Bézard et al. 1997) or 5.6×10^{-5} (Orton et al. 1992) for Neptune and 5.5×10^{-5} (Feuchtgruber et al. 1999) in Uranus, possibly as a consequence of the inclusion of highly deuterated icy planetesimals into the planets as they formed.

In our previous paper (Willacy 2007), we considered the deuterium chemistry in the outer regions ($R > 50$ AU) of a protostellar disk. We showed that although the gas-phase molecular D/H ratios can be considerably altered by chemical processing in the disk, the grain mantle ratios reflect those set in the parent molecular cloud, supporting the idea that comets may contain interstellar material that survived the formation of the Sun and planets relatively unchanged. Here we extend our previous work to cover the inner disk from 0.5 to 30 AU. This radius range covers the comet and planet forming region, and is also appropriate for comparison to infrared observations of the inner regions of protostellar disks.

We present the results for a typical T Tauri star disk and for a more massive disk with a higher surface density similar to the minimum mass solar nebula (MMSN). Our models include multiply deuterated molecules since in high-density regions these can become important (Ceccarelli & Dominik 2005; Roberts et al. 2002, 2003) although their effects in the warm inner disk are expected to be less than in the colder outer disk. We compare our results with the available observations of the inner disk (non-deuterated molecules) and with observations of deuterated molecules in comets.

2. THE MODEL

To fully model a disk self-consistently requires many chemical and physical processes to be taken into account. To simplify this process and to reduce the required computing time we separate the calculation of the physical structure of the disk from the chemical network. We obtain the disk structure (density and grain temperature) from a pre-existing hydrodynamical model (d'Alessio et al. 1999, 2001). These models use the α prescription to determine the density and temperature distribution throughout the disk.

We consider two of d'Alessio's models with different mass accretion rates. The first (Model 1) has $\dot{M} = 10^{-8} M_\odot$ yr^{-1}, a central star of mass $M_* = 0.7\ M_\odot$, radius $R_* = 2.5\ R_\odot$, luminosity $L_* = 0.9\ L_\odot$, and temperature $T_* = 4000$ K. The viscosity parameter α is 0.01. The dust distribution is described by a power law $n(a) = n_0 a^{-p}$ where a is the grain radius, and $p = 3.5$. The maximum grain size is 0.25 μm and the dust is assumed to be well mixed with the gas. The surface density at 5 AU is 38.8 g cm^{-2}. This model is the same as used in Willacy (2007, hereafter W07) and so represents a continuation of the model to smaller radii.

The mass of the disk in this model is somewhat lower than that expected in the early solar system. We, therefore, also consider a more massive disk (Model 2) where the surface density is closer to that of the MMSN (Hayashi 1981). In this model, $\dot{M} = 10^{-8}\ M_\odot$ yr^{-1} and $\alpha = 0.025$. All other parameters remain the same as in Model 1. The surface density at 5 AU for Model 2 is 150 g cm^{-2}.

Although the hydrodynamical models assume that the gas and grain temperature are equal, this is not the case in the surface layers of the disk, e.g., Kamp & Dullemond (2004); Gorti & Hollenbach (2004), where the gas temperature can be much higher than the grain temperature. Since the gas temperature can critically affect the chemical (and especially the isotopic) abundances, we elect to calculate the gas temperature separately. This calculation is based on the work of Kamp & Dullemond (2004) and is described in more detail in Woods & Willacy (2009). We summarize here the processes that are included. Heating is provided by the photoelectric effect, photodissociation of H_2, the formation of H_2 on the surfaces of dust grains, the ionization of carbon atoms, cosmic rays, and stellar X-rays. Gas–grain collisions can also act as heating processes in regions where the grains are hotter than the gas, but this is not an important process in the inner disk, where this process is more likely to cool the gas. Cooling occurs via the emission lines of atomic oxygen and carbon, C^+, CO and CH, and by Lyα cooling. The rates for these processes are given in Woods & Willacy (2009).

For H_2 formation heating, we use the H_2 formation rate from Cazaux & Tielens (2002), which assumes that H atoms can both chemisorb and physisorb to bare grains. Chemisorption only occurs on bare grains, and this rate is therefore only valid at the top of our disk. Below this where the grains are covered in ices, we assume that only physisorption occurs with the binding energy given in Cazaux & Tielens (2002). This results in cooler temperatures than were found by Kamp & Dullemond (2004) in regions just below the disk surface where ices have begun to form. Figure 1 shows the density and temperature distributions for the two models used.

The final parameter required is the UV field. In order to estimate the UV field in the disk, we adopt the model of Richling & Yorke (2000) which uses a ray tracing method and the flux limited diffusion approximation to determine the field at each point in the disk. This allows us to model the effects of UV irradiation by the interstellar UV field, and by the central protostar and to include scattering of the UV photons by dust grains. The grain absorption and scattering coefficients

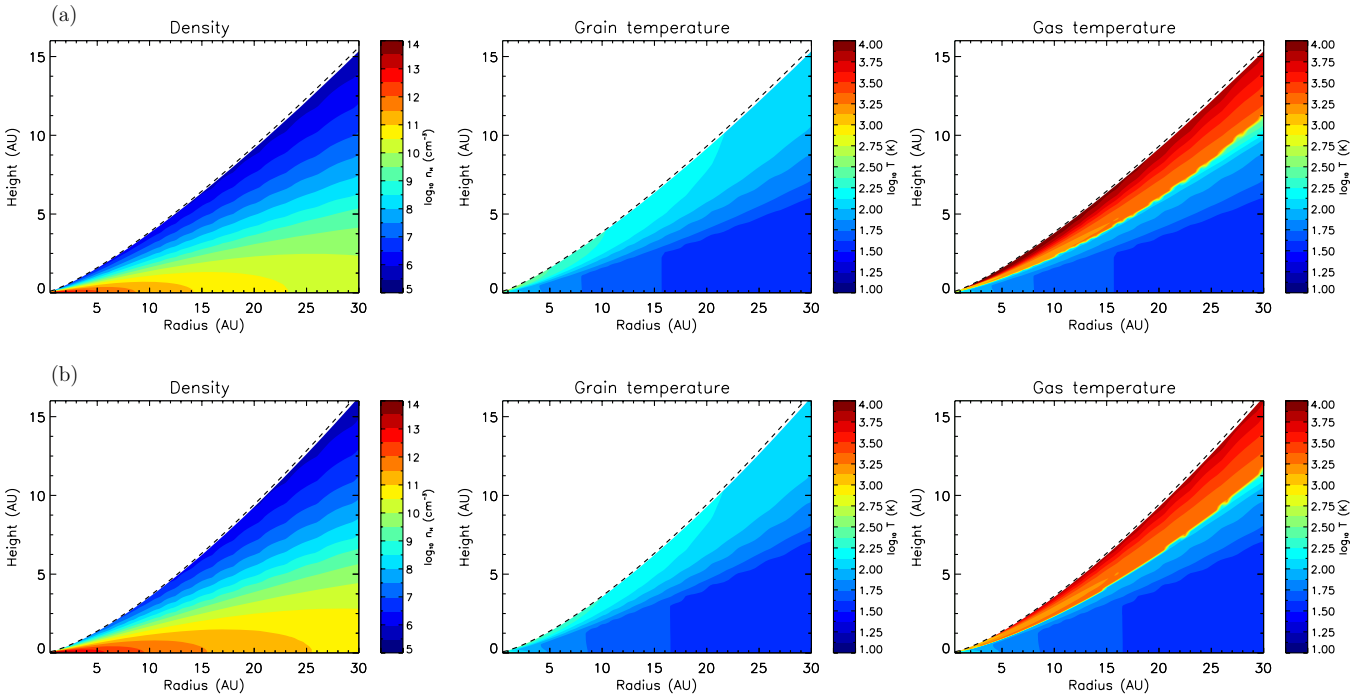

Figure 1. Physical parameters used in (a) Model 1 ($\alpha = 0.01$) and (b) Model 2 ($\alpha = 0.025$). Left: the gas density; center: the grain temperature; right: the gas temperature. Gas density and grain temperature are supplied by the models of d'Alessio, and the gas temperature is calculated separately by balancing the heating and cooling processes.

(A color version of this figure is available in the online journal.)

are based on Draine & Lee (1984) and Preibisch et al. (1993) who assumed a mixture of silicates, amorphous carbon and dirty ice-coated silicate grains. The disk is divided into square cells ($\Delta z = \Delta R = 0.02$ AU) and the radiative transfer equation is solved separately for both sources of radiation and for the direct and diffuse (scattered) components of each field (see Richling & Yorke 2000, for details). The total UV flux at a given point is the sum of the contributions from the stellar and interstellar fields. In general, this results in a total UV field that is higher than that estimated from our previous slab method: see, for example, W07. A similar effect was found by van Zadelhoff et al. (2003) for a more complex radiative transfer model in the outer disk.

Using the density and temperature distributions provided by the d'Alessio disk model, we calculate the UV field for both the interstellar and stellar fields. For the latter, we assume that the UV field emitted by the T Tauri star is 500 G_0 at 100 AU where G_0 is the standard interstellar radiation field (ISRF). This field strength is based on observations of T Tauri stars by Bergin et al. (2003), but we do not take into account the possibility that the T Tauri spectrum has a different shape to the ISRF and that it may be dominated by strong emission features such as Lyα. This can significantly impact the chemistry of the surface layers of the disk since Lyα can dissociate some molecules such as OH and CH_4, but not others. Bergin et al. (2003) found that this effect can account for high CN/HCN ratios observed in some disks (Dutrey et al. 1997; Kastner et al. 1997).

Following previous authors (e.g., Woods & Willacy 2009; Markwick et al. 2002; Willacy et al. 1998) we assume that material advects inward toward the star. We do not have a completely integrated dynamical and chemical model and instead follow parcels of gas, starting at the outer edge of the disk (in this case 35 AU) which gradually move inward. The parcels move inward in discrete radial steps of 0.5 AU and travel along lines of constant gas pressure scale height. The time that a gas parcel remains at a given grid position can be determined from the radial velocity:

$$v_r = \frac{\dot{M}}{2\pi\Sigma R}, \tag{1}$$

where Σ is the surface density of the disk at radius, R. The timescale for accretion, $\Delta t \approx \Delta R/v_r$, and therefore the time that a parcel of gas spends at each radius is given by

$$\Delta t \sim \frac{2\pi\Sigma R\Delta R}{\dot{M}}. \tag{2}$$

Σ scales roughly with $1/R$ for $R > 10$ AU (d'Alessio et al. 2001) so Equation (2) has only a small dependence on R. Starting at 35 AU, a parcel of gas will migrate into the star in approximately 0.41 million years. In our grid, the parcel spends roughly 6000 years at each radius before moving inward to the next gridpoint. We have 70 radial and 56 vertical grid positions.

2.1. The Chemical Network

Our chemical network is the same as used by W07. We take the basic gas-phase reaction set from the UMIST database RATE95 (Millar et al. 1998) and add deuterated reactions using the techniques of Millar et al. (1989) and Rodgers & Millar (1996). The reaction rates for the multiply deuterated isotopologues of H_3^+ and CH_3^+ are taken from Roberts et al. (2004). For details of the grain surface chemistry, see W07. The reaction network links 227 gas-phase species (of which 115 are deuterated) and 91 grain species (44 of which are deuterated) by 9489 reactions.

We also include freezeout, thermal desorption, and cosmic ray heating of grains. The rate at which a species, X, will freeze out onto dust grains is given by

$$k_{\rm freeze} = S_X C_X \langle \pi a^2 n_g \rangle \, v_X \ {\rm s}^{-1}, \tag{3}$$

Table 1
The Binding Energies (E_D) Used to Determine the Thermal Desorption Rates of the Abundant Mantle Species

Species	E_D (K)	Reference	Species	E_D (K)	Reference
H	600	1	D	621	2
H_2	315	8	C	800	3
CH	645	9	CH_2	956	9
CH_3	1158	9	CO	855	4
CO_2	2860	5	H_2CO	1760	3
CH_3OH	4240	7	O	800	3
O_2	1210	3	OH	1259	9
H_2O	5770	6	N	800	3
N_2	790	4	NH	604	9
NH_2	856	9	NH_3	3080	5

References. (1) Cazaux & Tielens 2002, 2004; (2) Caselli et al. 2002; (3) Tielens & Allamandola 1987; (4) Öberg et al. 2005; (5) Sandford & Allamandola 1990; (6) Fraser et al. 2001; (7) Sandford & Allamandola 1993; (8) Ruffle & Herbst 2000; (9) Allen & Robinson 1977.

where S_X is the sticking coefficient (= 0.3 for all species), a is the grain radius, n_g is the number density of grains, and v_X is the gas-phase velocity of X. C_X is a factor to take into account the increase in freezeout rate for positive ions encountering a negatively charged grain (Umebayashi & Nakano 1980). C_X is 1 for neutral species, and $1 + 16.71 \times 10^{-4}/(aT_{gr})$ for positive ions, where T_{gr} is the grain temperature. Ions are assumed to recombine on the grain surface in the same way as they do when reacting with electrons in the gas. All species are assumed to freeze out with the exception of He and He^+ which have a very low binding energy and are easily thermally desorbed even at low temperatures. Any He^+ that hits a grain is immediately returned to the gas as neutral He.

The thermal desorption rate is given by

$$k_{\rm therm} = \nu_0 e^{-E_D/T_{gr}}\ {\rm s}^{-1}. \quad (4)$$

ν_0 is the frequency of oscillation between the absorbate and the grain surface, and is given by

$$\nu_0 = \sqrt{(2n_s E_D/\pi^2 m)}, \quad (5)$$

where n_s is the surface density of sites ($\sim 1.5 \times 10^{15}$ cm^{-2}), m is the mass of the accreting species, and E_D is its binding energy. The binding energies used are summarized in Table 1. For deuterated species, the binding energies are assumed to be 21 K more than their undeuterated equivalents (21 K is the difference in zero-point energy between the hydrogen and deuterium atoms) (Caselli et al. 2002). For example, $E_D(H_2O)$ = 5770 K, E_D(HDO) = 5791 K and $E_D(D_2O)$ = 5812 K. Binding energies for species not listed in Table 1 are taken from Hasegawa & Herbst (1993) and Hasegawa et al. (1992).

Cosmic ray heating can remove weakly bound molecules from grains in regions where the temperatures are low, and where the surface density of the disk is low enough that cosmic rays can penetrate. The desorption rates due to cosmic ray heating are taken from Hasegawa & Herbst (1993) using updated binding energies for some species, e.g., CO (Öberg et al. 2005).

In our outer disk models (W07), we included photodesorption since at $R > 50$ AU the grain temperatures are low enough that thermal desorption is not efficient for most species. Photodesorption was found to remove molecules in the surface layers of the disk even when the grain temperature was low. In the inner disk model, the grain temperatures in the surface layers are warm enough that even the molecules with the highest binding energies can be removed efficiently by thermal desorption and therefore photodesorption will have little effect on the molecular abundances. Hence we have chosen to exclude it from our current models.

2.1.1. Ionization Processes

Ionization in the disk can arise from several processes including irradiation by UV photons (both interstellar and stellar), protostellar X-rays and cosmic rays. There is also a contribution from the decay of radioactive isotopes.

The UV field at each disk position is calculated as described in Section 2. The stellar field is taken to be 500 G_0 at 100 AU (Bergin et al. 2003) where G_0 is the ISRF. We assume that the stellar field does not dissociate CO and H_2 (Aikawa et al. 2002), although these molecules are dissociated by the interstellar field. We calculate the self-shielding of CO and H_2 using the slab model of Lee et al. (1996). This model was developed for molecular clouds and provides data for the shielding due to H_2, CO and dust as a function of column density. The line widths assumed are 3 km s^{-1} which is much larger than that observed in disks, where the velocity dispersion in the outer disk, at least, is almost thermal (Guilloteau & Dutrey 1998). To take account of this we have followed Aikawa & Herbst (1999) in scaling the column densities in Table 10 of Lee et al. by c_s/3 km s^{-1} where c_s is the local sound speed in the disk. This scaling factor is only required for H_2 since the CO dissociation lines are broader due to predissociation.

HD does not self-shield, but some of its lines do overlap with those of H_2. This means that H_2 can provide some shielding. Barsuhn (1977) estimated this would reduce the HD photodissociation rate by 1/3, assuming that the overlapped HD lines are totally shielded by H_2. Here we modify the HD dissociation rate accordingly.

Cosmic rays can also cause ionization, both directly and indirectly (by interaction with H_2 producing UV photons). The rates for both processes are taken from the UMIST ratefile, with an assumed cosmic ray ionization rate $\zeta_0 = 1.3 \times 10^{-17}$ s^{-1}. Cosmic rays can produce ionization in the disk only if the surface density (Σ) is low enough for them to penetrate, i.e., Σ is less than 150 g cm^{-2} (Umebayashi & Nakano 1981). We assume that cosmic rays only penetrate the disk vertically, and that they can penetrate from both above and below the disk. Their ionization rate is given by

$$\zeta_{\rm CR} = \tfrac{1}{2}\zeta_0[\exp(-\Sigma_1(z, R)/10^2) + \exp(-\Sigma_2(z, R)/10^2)] \quad (6)$$

(Semenov et al. 2004), where Σ_1 is the surface density between the height above the midplane, z, and the top of the disk, and Σ_2 is the surface density between z and the bottom of the disk.

The decay of radioactive nuclides is an additional source of ionization. ^{26}Al can decay to form excited ^{26}Mg, which in turn decays by either positron decay or by electron capture. The ionization rate of these processes is assumed to be $\zeta_{\rm Al} = 6.1 \times 10^{-19}$ s^{-1} (Umebayashi & Nakano 1981).

A final source of ionization is X-rays of which T Tauri stars are strong emitters. We use the approach of Gorti & Hollenbach (2004) to calculate the X-ray photoionization rates of atoms and molecules. This method assumes that the X-ray photoionization rate of a molecule is the sum of the rate for its constituent atoms and that X-ray ionization leads to the loss of a single electron. The ionization rate per atom depends on the incident X-ray flux and the cross section of the atom. We calculate fits to

Table 2
Elemental Abundances Used in the Model

Element	Abundance $n(x)/n_H$
H_2	0.495
H	0.01
He	0.14
D	1.6×10^{-5}
O	1.76×10^{-4}
C	7.3×10^{-5}
N	2.14×10^{-5}
Fe	3.0×10^{-9}
Mg	7.0×10^{-9}

Notes. Abundances are given with respect to the total abundance of hydrogen atoms, $n_H = 2\ n(H_2) + n(H)$. Initially, we assume that 1% of the hydrogen is atomic, with the rest molecular, and that 1% of the deuterium is atomic, with the rest in HD.

the energy-dependent atomic cross sections given in Verner & Yakovlev (1995). The attenuation depth of X-rays is very small and X-ray ionization is most efficient in the surface layers of the disk. For further details, see Woods & Willacy (2009).

2.2. Recombination of N_2H^+

The recombination of N_2H^+ with electrons has recently been the subject of study in the laboratory with two different groups producing two different results. There are two possible pathways for this reaction:

$$N_2H^+ + e^- \longrightarrow NH + N \quad (7)$$

$$\longrightarrow N_2 + H. \quad (8)$$

The pathway followed by this reaction can influence the abundance of nitrogen-bearing molecules in the gas phase. If the primary product is NH, then in cold regions of the disk, NH will quickly freeze out and be converted to NH_3 ice, removing nitrogen from the gas phase. N_2, on the other hand, does not react on the grains and is relatively easy to desorb. N_2 is also an important means of controlling the degree of ionization (Ceccarelli & Dominik 2005). The presence of N_2 in the gas can prevent the transfer of deuteration along the chain of isotopologues from H_3^+ to D_3^+ by destroying the less deuterated isotopologues before they have a chance to form D_3^+.

In W07, we took the results of Geppert et al. (2004) which found that the NH route is most likely to happen, occurring 65% of the time. However, more recent laboratory work from Molek et al. (2007) has cast some doubt on this result. Molek et al. (2007) found that the route leading to N_2 dominates, with no significant NH being formed.

Using the Geppert et al. results leads to lower abundances of N_2 in the midplane compared to models using Molek et al. This will translate into a higher deuteration of H_3^+ and lower abundances of gas-phase nitrogen molecules.

Here we use the more recent results of Molek et al. and assume that little NH is formed by the recombination of N_2H^+.

2.3. The Initial Conditions

We assume that the material incorporated into the disk has first been processed to some extent in the parent molecular cloud. The input abundances for the disk model are therefore taken from the output of a molecular cloud model. The latter uses the elemental abundances found in Table 2 and is allowed to run for 1 Myr at a total hydrogen density $n_H = 2 \times 10^4$ cm^{-3}, temperature = 10 K and visual extinction $A_V = 10$ magnitudes. All the chemical processes included in the disk model are also included in the molecular cloud model with the exception of ionization by the decay of radioactive nuclei. The input disk abundances are given in Table 3. The processes that drive deuteration chemistry in molecular clouds have been well described by previous authors, e.g., Roberts et al. (2004); Roberts & Millar (2000); Charnley et al. (1997); Brown & Millar (1989); Tielens (1983).

Table 3
Input Fractional Abundances with Respect to Total Number of Hydrogen Nuclei for the Disk Model as Determined by a Molecular Cloud Model at 1 Myr

Molecule	Abundance		Molecule	Abundance	
	Gas	Grain		Gas	Grain
H	2.8 (−5)	...	D	6.7 (−7)	...
H_3^+	3.0 (−9)	...	H_2D^+	5.8 (−10)	...
HD_2^+	9.8 (−11)	...	D_3^+	1.5 (−11)	...
CO	3.2 (−5)	2.7 (−6)	CO_2	5.8 (−8)	2.2 (−7)
HCO^+	3.5 (−9)	...	DCO^+	3.1 (−10)	...
H_2CO	2.4 (−7)	1.6 (−6)	HDCO	1.6 (−8)	7.7 (−8)
CH_3OH	1.6 (−10)	4.0 (−8)	CH_3OD	9.3 (−12)	9.1 (−10)
CH_2DOH	1.5 (−11)	3.2 (−9)	O	8.5 (−7)	...
O_2	4.4 (−8)	...	OH	2.4 (−8)	...
OD	4.1 (−8)	...	H_2O	3.8 (−8)	1.4 (−4)
HDO	3.8 (−9)	1.2 (−6)	D_2O	4.2 (−11)	1.3 (−8)
N	1.0 (−7)	...	N_2	1.9 (−6)	6.5 (−8)
NO	4.5 (−8)	...	CN	6.6 (−8)	...
HCN	2.1 (−8)	2.4 (−6)	DCN	6.7 (−10)	2.0 (−8)
HNC	9.9 (−9)	1.1 (−7)	DNC	3.9 (−10)	2.1 (−9)
HC_3N	2.5 (−7)	9.9 (−7)	DC_3N	9.4 (−9)	3.3 (−8)
NH_3	8.6 (−9)	1.3 (−5)	NH_2D	2.7 (−10)	6.7 (−8)
NHD_2	5.1 (−12)	3.1 (−10)	ND_3	8.7 (−13)	2.1 (−11)
N_2H^+	2.8 (−10)	...	N_2D^+	2.8 (−11)	...
C	3.9 (−7)	...	C^+	3.1 (−9)	...
C_2H	6.4 (−9)	...	C_2H_2	1.1 (−7)	3.3 (−7)
CH_4	3.1 (−6)	1.1 (−5)	CH_3D	1.6 (−7)	3.4 (−7)
CH_2D_2	6.1 (−9)	1.8 (−8)	CHD_3	1.5 (−10)	5.0 (−10)
CD_4	8.2 (−13)	2.1 (−12)	HD	1.2 (−5)	...

Notes. The results for two models are shown. The numbers vary a little from those in Table 3 in W07 because of the use of the Molek et al. (2007) results for N_2H^+ recombination instead of Geppert et al. (2004). The physical parameters used were density, $n_H = 2 \times 10^4$ cm^{-3}, temperature = 10 K, and $A_V = 10$ magnitudes. Freezeout, thermal desorption and cosmic ray heating of grains were included. Grain chemistry contributes to the formation of some of the ice molecules, e.g., water, whereas others, e.g., CO, form in the gas phase and then freeze out but are not produced in situ on the grain surfaces.

3. RESULTS

In common with previous authors, e.g., Aikawa & Herbst (1999); Willacy & Langer (2000); Aikawa et al. (2002); van Zadelhoff et al. (2003) we find that the disk can be divided vertically into three chemically distinct layers. Grains are coldest in the midplane, leading to the existence of ices of at least some species at $R > 2$ AU. Inside of 2 AU, the grains are hot enough that all molecules are desorbed in the midplane. Above the midplane is a molecular layer where thermal desorption is efficient and the disk is sufficiently optically thick that molecules can survive in the gas phase. This leads to high gas-

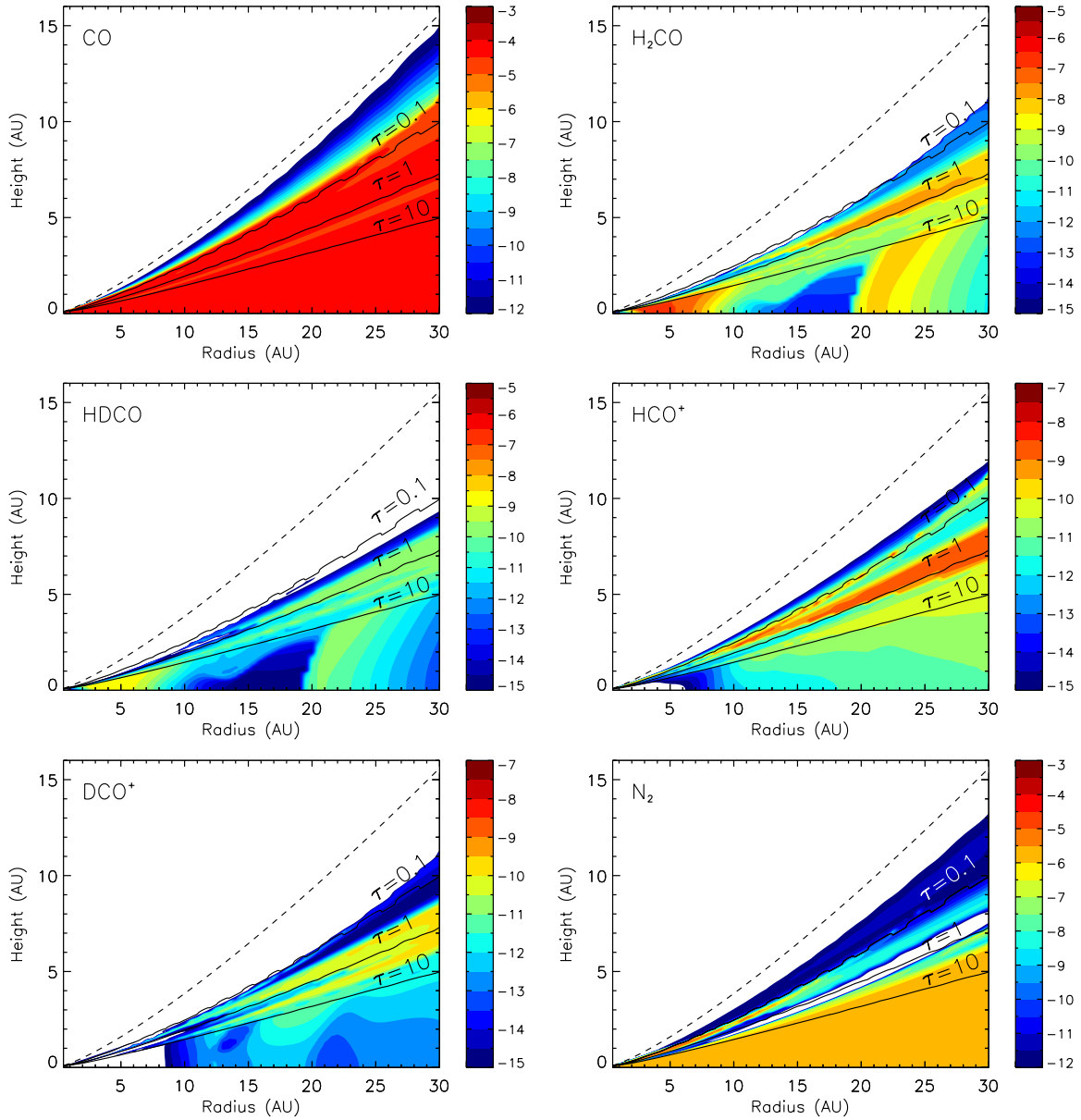

Figure 2. Fractional abundances in the inner disk for Model 1 ($\alpha = 0.01$). Note the change of radial scale for molecules that are only abundant in the inner few AU, i.e., H_2O, HDO, NH_3, and NH_2D. The dashed line indicates the surface of the disk (at 6 pressure scale heights above the midplane). Also marked are optical depths, τ, of 0.1, 1, and 10.

(A color version of this figure is available in the online journal.)

phase molecular abundances. In the surface layer, UV and X-rays can penetrate, dissociating molecules into their constituent atoms and ions. The distinction between the midplane and the molecular layer is not as clear as that seen in outer disk models, since the grains are warm enough even in the midplane for some volatile species (e.g., CO and N_2) to desorb. We use these three layers in the discussions below.

Figure 2 shows the fractional abundance distributions in the inner disk. The abundance distribution is a combination of the effects of the formation and destruction processes at a given radius, together with the transport to that radius of molecules formed further out in the disk. Many molecules desorb as their sublimation temperature is reached and then show little variation in their gas-phase abundance with radius, e.g., N_2 and CO show no significant change in abundance across the inner 30 AU of the disk below the surface photodissociation layer. The upper extent of these molecules is determined by photodissociation. N_2 shows a more complicated behavior than CO, with a low abundance region (where $x(N_2) < 10^{-12}$). Here photodissociation is still efficient and the resulting nitrogen atoms are incorporated into other nitrogen-bearing molecules, e.g., HCN. HCN has a high binding energy of 4173 K and the grain temperature in this region is low enough that once HCN freezes out it is not able to thermally desorb. This leads to a loss of nitrogen atoms from the gas and hence N_2 cannot reform. Above the low-abundance layer, HCN still forms from nitrogen atoms, but the difference is that the grains are warm enough for desorption of HCN to be efficient. Hence nitrogen atoms can cycle between N_2 and HCN. Below the low-abundance region N_2 does not photodissociate and has a high abundance.

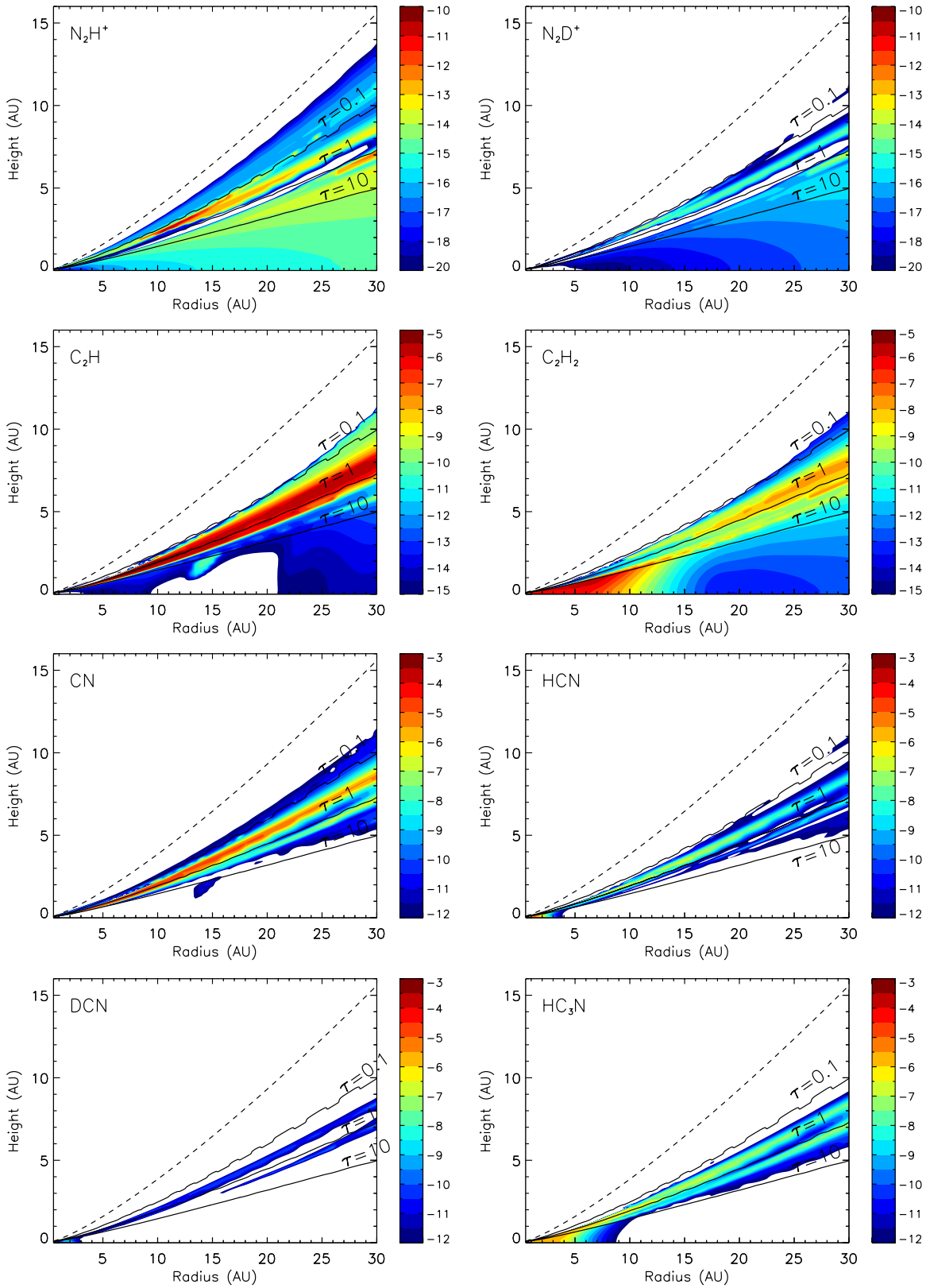

Figure 2. (Continued)

The effects of an increase in temperature toward the disk surface and toward the star can be seen in the increase in abundance of less volatile species such as H_2O and HCN in these regions. Ammonia has a lower binding energy and is present for a larger radial extent than either H_2O or HCN, but it does not survive in the surface layers where it is quickly destroyed by reaction with abundant CN, producing HCN. The HCN freezes out and is retained on the grains and NH_3 is not reformed. NH_3 only exists in regions shielded from UV radiation.

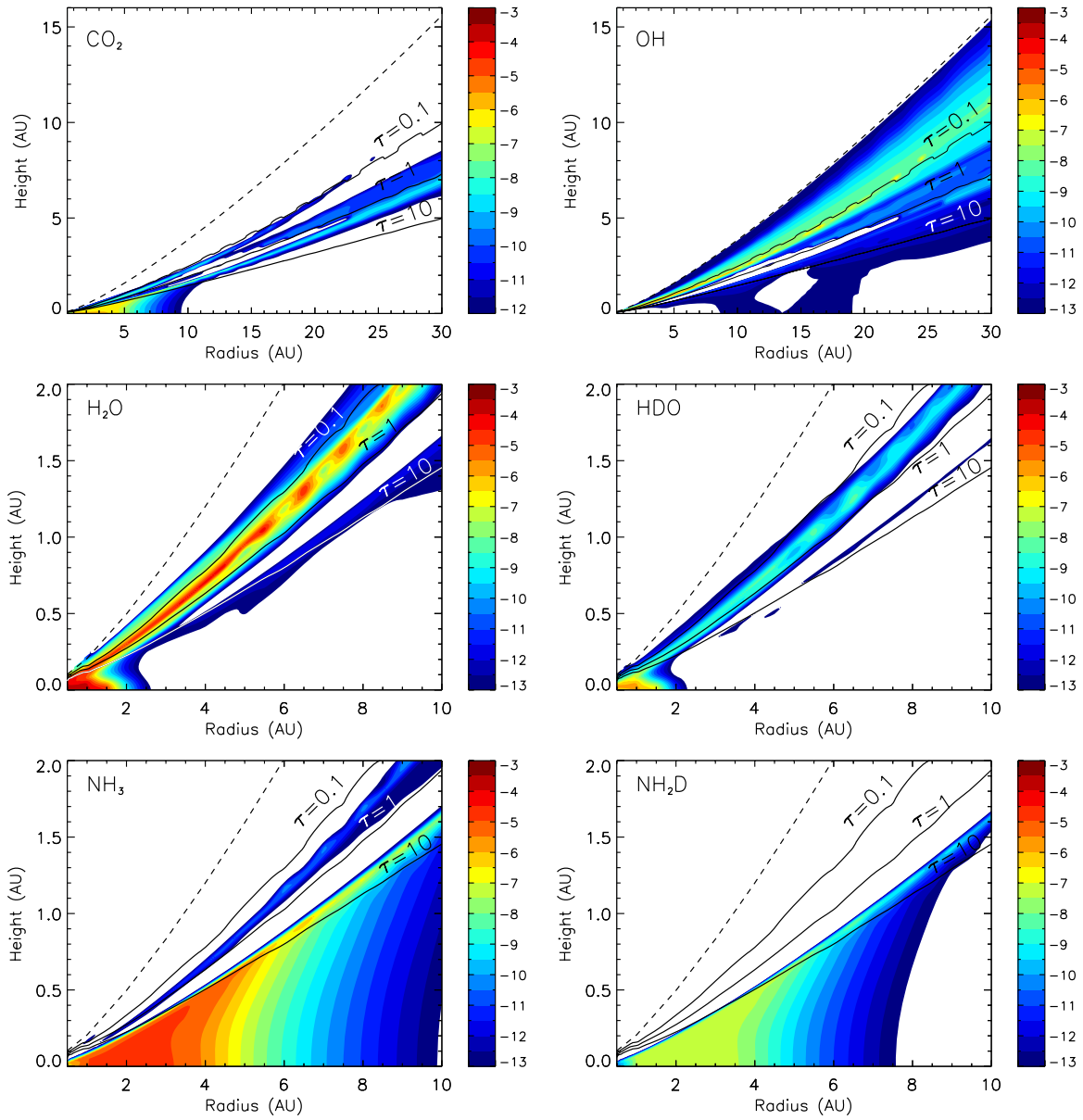

Figure 2. (Continued)

H_2CO shows two abundance peaks in the midplane, as well as a peak in the molecular layer above it. The outermost midplane peak (at $R = 20$–23 AU) and the molecular layer peak are due to thermal desorption. Between 7 and 20 AU, H_2CO is quickly destroyed by gas-phase reactions with HCO^+ and DCO^+ followed by neutralization of the resulting ions (H_3CO^+ and H_2DCO^+) either with electrons or on grain surfaces. While some of the ions will reform H_2CO, 1/3 will instead form CO, leading to a removal of H_2CO from the gas.

The second peak at $R < 8$ AU is due to formation in the gas phase by

$$O + CH_3 \longrightarrow H_2CO + H. \quad (9)$$

The oxygen atoms are supplied by the destruction of CO by reaction with He^+. CH_3 is supplied by the breakdown of C_3H_4 (which is desorbed at $\sim$ 7 AU). HDCO forms by similar processes.

C_2H exists in the boundary between the molecular and surface layers as a photodissociation product of C_4H_2 at $R > 10$ AU and of HC_3N inside of this radius.

The abundances of molecular ices do not vary much across the disk, until their desorption temperature is reached. The ice abundances are set by reactions in the molecular cloud and are not altered by grain chemistry in the disk.

3.1. Gas-phase Column Densities

Figure 3 shows the radial variation in column density measured vertically from the midplane for some molecules as calculated in Model 1. Most molecules show a sharp increase in column density due to thermal desorption as the radius decreases, e.g., HCN, CO_2, NH_3. A corresponding increase in fractional abundance can be seen for these molecules in Figure 2. The increase in the column density of the equivalent deuterated molecules occurs at slightly smaller radii because of their slightly higher binding energies. The fall in DCN at $R <$ 1.5 AU is because of its reaction with hydrogen atoms to form HCN. The reverse reaction (D + HCN $\longrightarrow$ DCN + H) can also occur, and at the same rate, but DCN does not reform because the atomic D/H ratio is low at small radii. N(CN) also increases

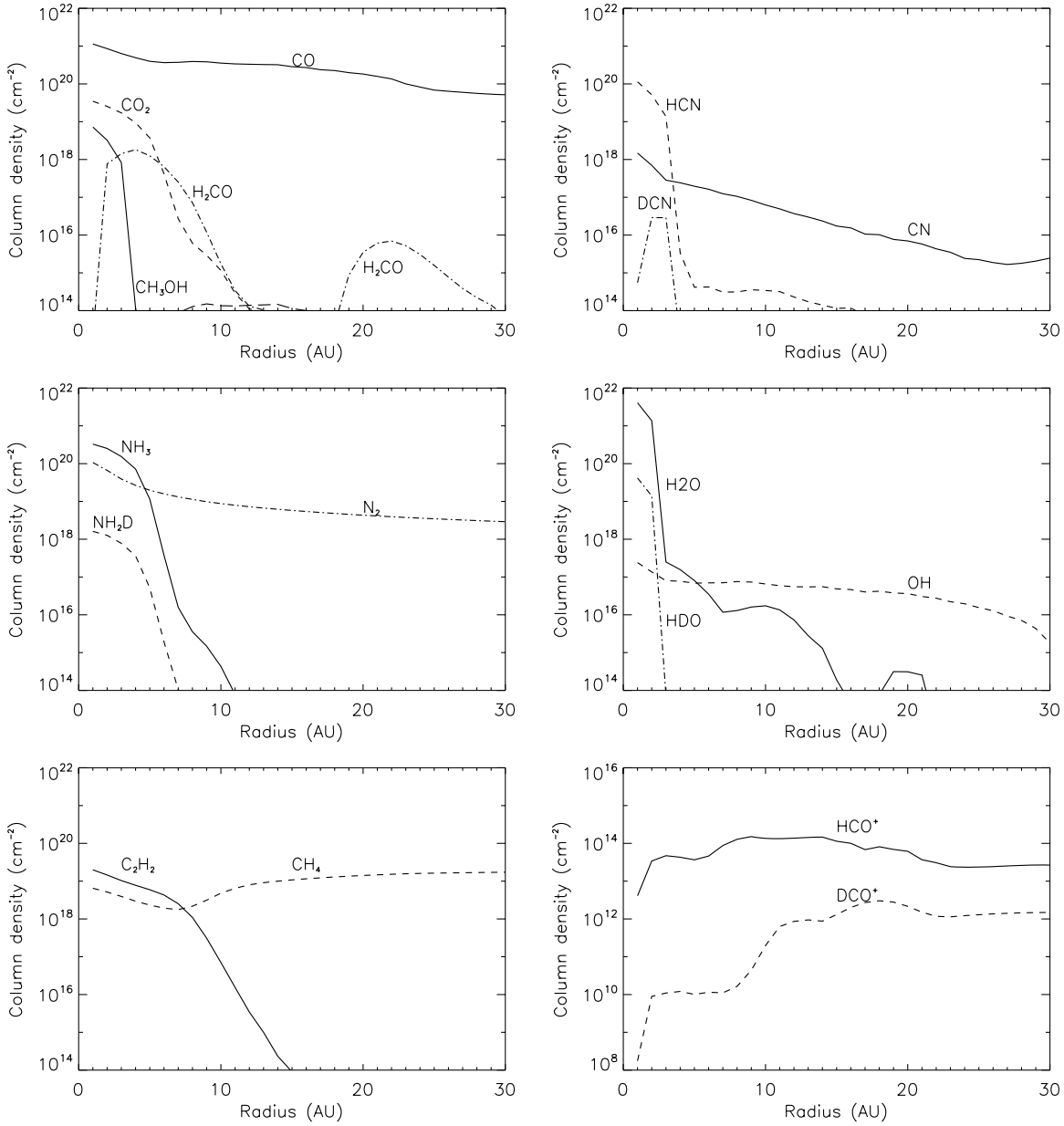

Figure 3. Calculated column densities in Model 1 of some molecules in the inner 30 AU.

closer to the star. It is a photodissociation product of DCN and HCN, and therefore exists mainly in the surface layers.

H_2CO shows two column density peaks: one around 23 AU and one around 3–4 AU corresponding to the fractional abundance peaks in the midplane seen in Figure 2.

3.2. Deuteration in the Inner Disk

In low-temperature regions such as molecular clouds, enhancements in molecular deuteration are driven by the reactions of H_2D^+, CH_2D^+, and C_2HD. These form by

$$H_3^+ + HD \leftrightharpoons H_2D^+ + H_2 + \Delta E_1$$
$$CH_3^+ + HD \leftrightharpoons CH_2D^+ + H_2 + \Delta E_2 \quad (10)$$
$$C_2H_2^+ + HD \leftrightharpoons C_2HD^+ + H_2 + \Delta E_3, \quad (11)$$

where ΔE_1, ΔE_2, and ΔE_3 are activation barriers, which inhibit the reverse reactions at low temperatures. ($\Delta E_1 = 220$ K at low temperatures, falling to ~ 130 K as the temperature increases, $\Delta E_2 \sim 370$ K and $\Delta E_3 \sim 530$ K. This allows deuteration to be transferred to other molecules via ion–molecule reactions. Roberts et al. (2003, 2004) showed that multiply deuterated forms of H_3^+, CH_3^+, and $C_2H_2^+$ also play an important role in determining the deuteration in cold regions. Grain surface reactions can also efficiently increase deuteration in ices, e.g., Tielens (1983); Brown & Millar (1989). For example, the high abundances of deuterated formaldehyde and methanol observed in star-forming regions (Parise et al. 2002; Loinard et al. 2002; Bacmann et al. 2003) have been attributed to the reaction of deuterium atoms on grains during an earlier low-temperature phase of evolution.

In our disk model, we find that the isotopologues of H_3^+ and CH_3^+ are the main drivers of deuteration with some contribution from the reaction of deuterium atoms. C_2HD^+ plays only a minor role. Figure 4 shows the fractional abundances of H_3^+ and

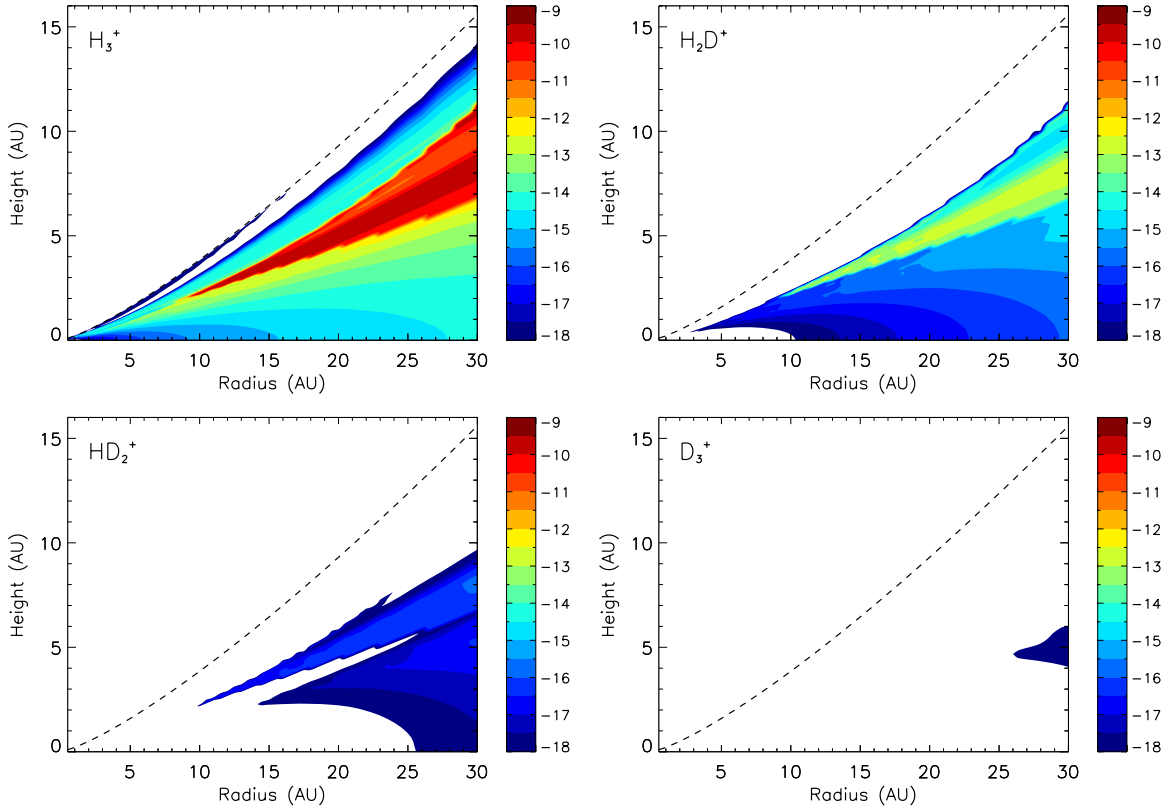

Figure 4. Fractional abundance distributions of the isotopologues of H_3^+ in a model with $\alpha = 0.01$.
(A color version of this figure is available in the online journal.)

its isotopologues, and the level to which this molecular ion is deuterated is shown in Figure 5. The abundance of H_3^+ peaks above the midplane where cosmic ray ionization is efficient and hydrogen is mainly atomic. But here the temperatures are relatively high, and the deuteration is low. In the midplane, the D/H ratios fall off rapidly with decreasing radius, and the more highly deuterated forms are present only at larger radii (Figure 5). In the outer disk ($R > 100$ AU), the models of W07 and Ceccarelli & Dominik (2005) found that HD_2^+ and D_3^+ are produced with significant abundances and therefore play an important role in the deuterium chemistry of this region. In the inner disk, the temperature is higher and the abundances of these isotopologues are much lower. Deuteration is therefore driven only by H_2D^+.

In common with H_3^+, the deuteration of CH_3^+ and atomic hydrogen peak in the midplane at $R > 15$ AU. The abundance of CH_3^+ is very small in this region, however, and its isotopologues play little part in driving the deuteration. Deuteration by reaction with atomic D is most efficient at $R > 17$ AU, and inside of 5 AU. The abundance of atomic D and H in the midplane is relatively high because of the high grain temperature. This reduces the residence time of the atoms on the grains so that they are more likely to desorb than to react with other atoms or radicals.

Other species do not necessarily show a decrease in D/H ratio with decreasing radius (and increasing temperature). Many molecules retain the D/H ratio that they had when they formed in the cold molecular cloud or in the colder regions of the disk, as they are transported inward. The transport process occurs on a shorter timescale than the chemical reactions that would destroy the deuteration. For example, the deuteration of H_2CO and NH_3 reflects that set in the ices during the molecular cloud phase and is not affected by chemistry in the disk.

The deuteration of gas-phase water is less than that seen in the ice. Water is desorbed in two regions, in the surface layers and at $R < 2$ AU. At high z HDO is formed by

$$OD + H_2 \longrightarrow HDO + H, \quad (12)$$

and destroyed by

$$HDO + H \longrightarrow OH + HD. \quad (13)$$

Similar reactions affect H_2O, but since the destruction product is OH, this is able to cycle back to form more water by reaction with H_2. Hence a decrease in HDO/H_2O is seen at high z. Below this, the ratio is higher (yellow stripe in Figure 6) but it is still lower than that set in the grain mantles, again due to the formation of OH from the destruction of HDO.

The increase in DCO^+/HCO^+ in the midplane between 20 and 10 AU is due to the increase in grain temperature which reduces the efficiency of H_2, HD, and D_2 formation on grains, and therefore increases the abundance of deuterium atoms in the gas phase. The deuterium atoms react with HCO^+ to form DCO^+. Inside of 10 AU the abundances of both DCO^+ and HCO^+ are very small because they are destroyed by reaction with hydrocarbons such as C_3H_4 and C_2H_2.

3.3. Ionization Fraction

Disks around young stars provide a means of dissipating angular momentum and they regulate the rate at which mass accretes onto the protostar. The evolution of the star–disk

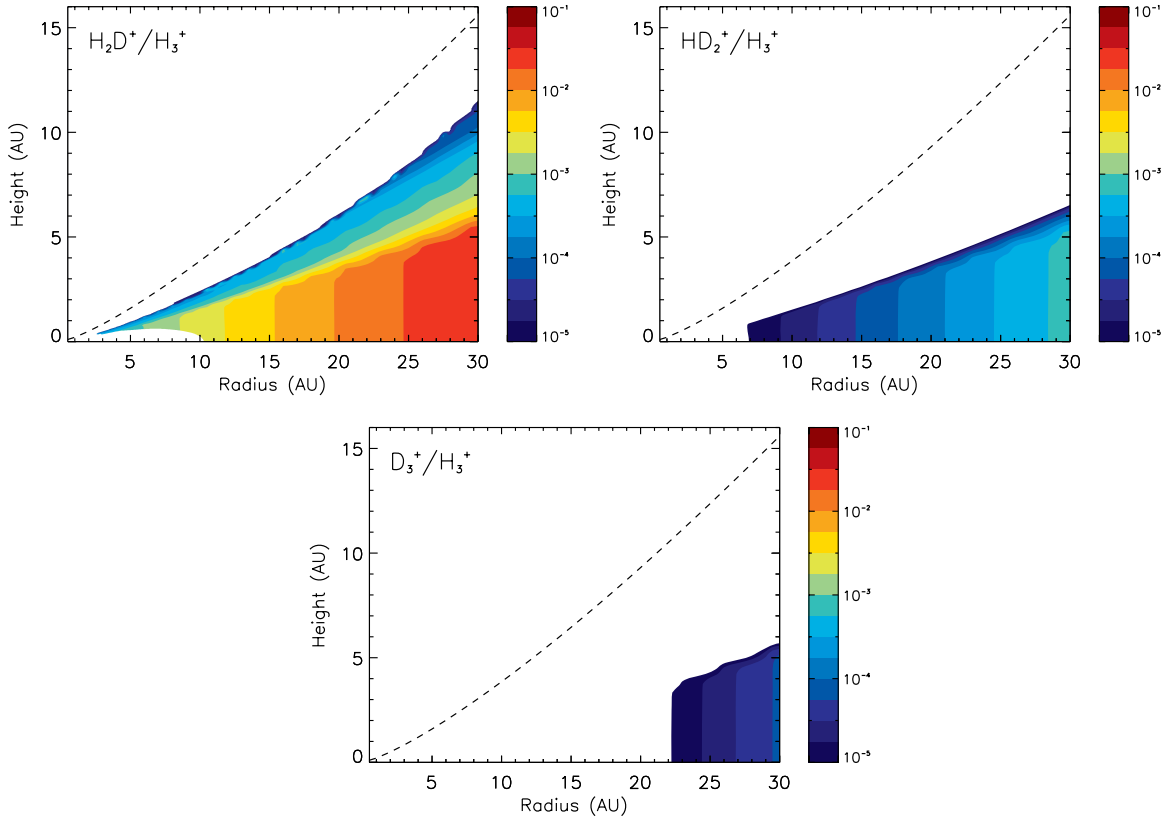

Figure 5. D/H ratios of the isotopologues of H_3^+ in Model 1.
(A color version of this figure is available in the online journal.)

system is controlled by angular momentum transport, but the> mechanism by which this is achieved is unclear. It is likely to involve turbulence (see Morfill & Völk 1984, and references therein) since molecular viscosity is too low to have much effect. The mechanism driving the turbulence has not yet been identified but several processes have been suggested, e.g., Lin & Papaloizou (1980); Ryu & Goodman (1982); Dubrulle (1993); Balbus et al. (1996); Balbus & Hawley (1991); Li et al. (2000); Klahr & Bodenheimer (2003); Klahr (2004); Dubrulle et al. (2005); Shalybkov & Rüdiger (2005). Magnetorotational instability (MRI) is widely regarded as the most promising mechanism for driving turbulence (Balbus & Hawley 1991; Hawley & Balbus 1991; Hawley et al. 1996). In MRI, magnetic field lines linking gas at different distances from the star are stretched due to the decrease in orbital frequency with radius. Magnetic tension forces decelerate the inner gas, which spirals inward and accelerates the outer gas, which spirals outward so that the bend in the field line grows with time. Instability occurs if the field lines are frozen in the gas. MRI requires the ionization fraction x(e) to be above a minimum value ($> 10^{-12}$ at 1 AU in the midplane of the MMSN; Inutsuka & Sano 2005). There is some debate as to whether MRI is applicable in disks, where high densities and low temperatures lead to low ionization levels (Blaes & Balbus 1994; Gammie 1996). Many models have found that active regions (where the ionization level is high enough to drive MRI) can exist in the disk along with dead zones where the magnetic field is not coupled to the gas, e.g., Sano et al. (2000); Fromang et al. (2002); Matsumura & Pudritz (2003); Semenov et al. (2004); Ilgner & Nelson (2006a, 2006b, 2006c). The size and location of the dead zone varies with the model, but most cover the region of terrestrial planet formation and it is thought that dead zones may also play a role in halting the inward migration of planets (Matsumura et al. 2007).

The total ionization level in Model 1 is shown in Figure 7(a). A dead zone (defined as a region where $x(e) < 10^{-12}$) is present in the midplane inside of $\sim$ 10 AU. The extent of the dead zone is sensitive to the mass of the disk—increasing the mass by increasing the value of α to 0.025 (Model 2) extends the dead zone out to 18 AU in the midplane (Figure 7(b)). This is a consequence of the higher densities in Model 2, which both increase the rate at which ions and electrons collide and neutralize and reduce the cosmic ray ionization rate in the midplane. The effects of an increase in disk mass on the abundance distributions of other molecules are discussed in Section 3.4.

The dominant ion varies with position in the disk. Figure 8 illustrates this for Model 1. At the surface, H^+ is the main ion at all radii. It is formed efficiently by X-ray ionization of H atoms. Below this is a layer of C^+ which lies above a thin layer of hydrocarbon ions, e.g., $C_4H_2^+$ and $C_3H_3^+$. The hydrocarbon ions dominate in a region where there are still some photons and where the high abundance of C^+ means that hydrocarbons and their ions can form efficiently. HCO^+ is the main charge carrier below the hydrocarbon layer for $R > 8$ AU. It is destroyed at $R < 8$ AU by reaction with hydrocarbon chains, e.g., C_3H_4 and C_2H_2 producing hydrocarbon ions that are the main contributors to the charge in the central regions. HCO^+ also contributes to the production of another abundant ion in the inner regions—CH_3CO^+—by reacting with CH_2CO.

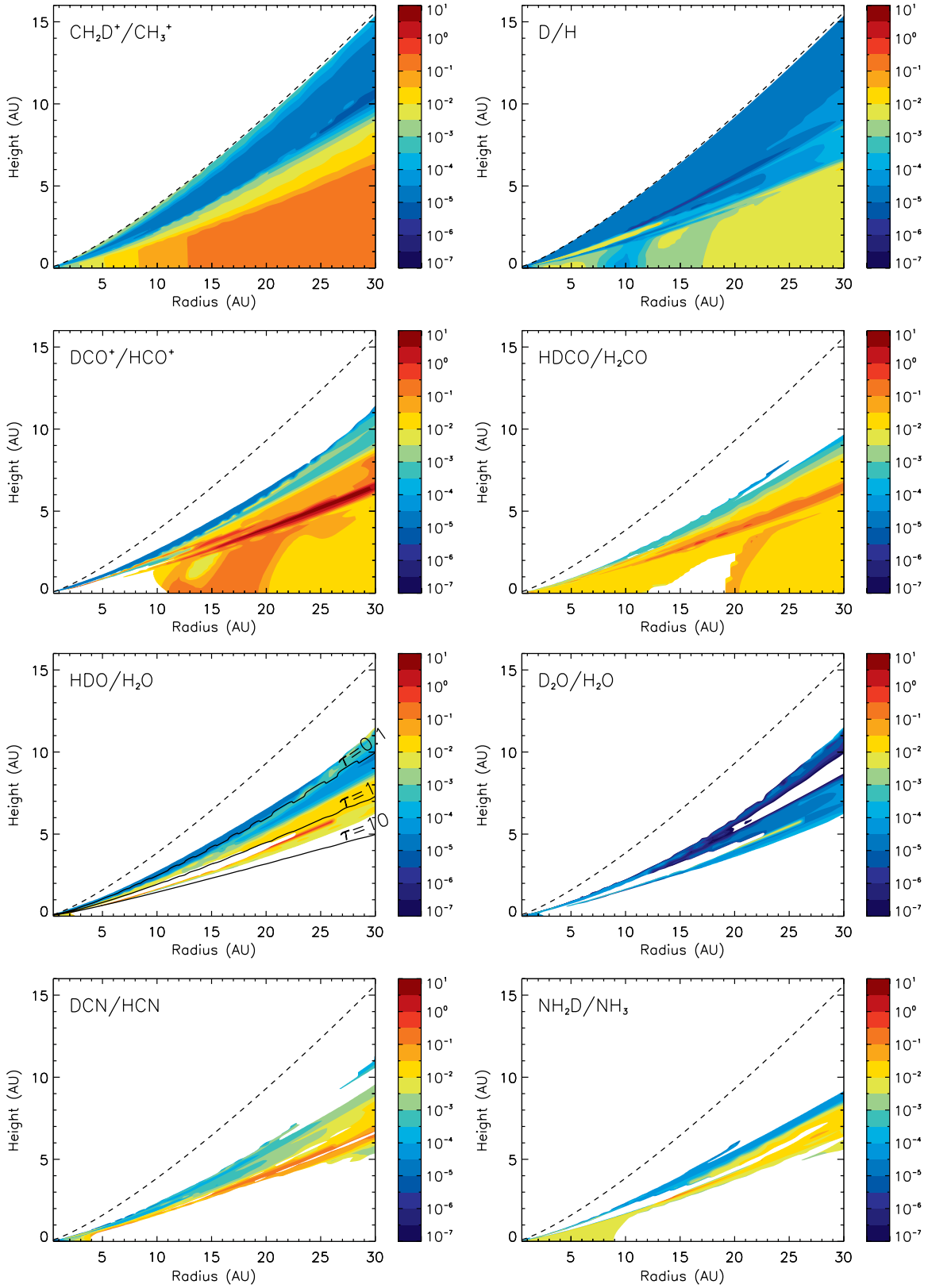

Figure 6. Molecular D/H ratios in the inner disk as calculated in Model 1. The D/H ratios are only shown in regions where the fractional abundance of the non-deuterated species is greater than 10^{-12} (the exception is CH_3^+ for which D/H ratios are shown across all of the disk regardless of the molecular abundances). Those species, which are abundant at $R > 10$ AU, have radial scales running from 0.5 to 30 AU. Other species are only shown for the inner 10 AU. The atomic D/H ratio and the CH_2D^+/CH_3^+ ratios are important for driving molecular deuteration of some molecules. Relatively high molecular deuteration is retained even in warm regions, since the ratios are set in the cooler outer regions of the disk and the material is transported inward at a faster rate than the chemical reactions that would destroy the deuteration.

(A color version of this figure is available in the online journal.)

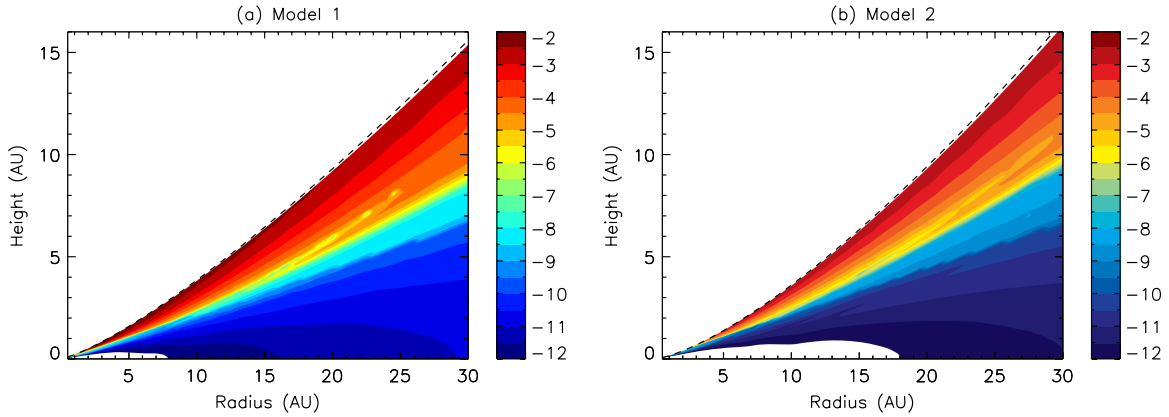

Figure 7. (a) Ionization level in disk of Model 1. A dead zone (defined as the region where $x(e) < 10^{-12}$) exists in the midplane at $R < 10$ AU; (b) the ionization level in the higher mass disk of Model 2, showing an increase in size of the dead zone with increasing disk mass.

(A color version of this figure is available in the online journal.)

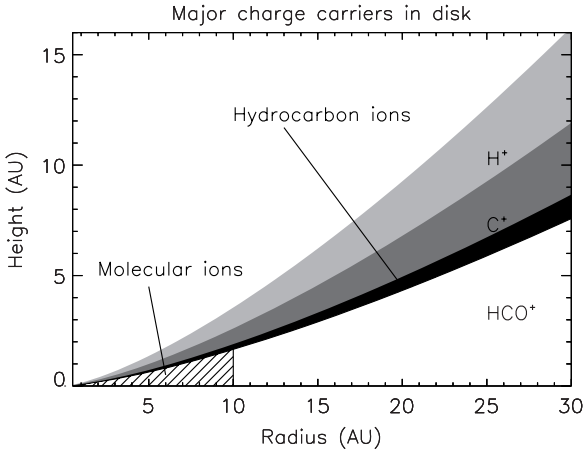

Figure 8. Distribution of ions in Model 1. HCO^+ is the dominant ion at $R > 8$ AU, CH_3CO^+ and hydrocarbon chain ions dominating inward of this. At the surface, the main ion is H^+, with a layer of C^+ below. Hydrocarbon ions exist in a layer below the C^+. A similar distribution is seen in Model 2.

3.4. Effect of Disk Mass

Model 1 described above has $\alpha = 0.01$ and a total disk mass of 0.032 $M_\odot$ inside of 300 AU. The surface density is 38.8 g cm^{-2} at 5 AU. This is somewhat lower than that of the MMSN model and we have therefore also considered a higher mass model, again provided to us by P. d'Alessio. Model 2 has a higher value of α (= 0.025) resulting in a higher surface density (150 g cm^{-2} at 5 AU).

We find that the mass of the disk does not greatly affect the molecular distributions in the inner disk (Figure 9). The higher mass does result in a narrower surface layer of molecules, e.g., for CN, H_2O, etc, and the slightly higher midplane grain temperature in Model 2 means that molecules desorb at slightly larger radii.

The deuteration of some molecules varies with the disk mass. Figure 10 shows the radial variation of column density deuteration for both models. HDO/H_2O and DCO^+/HCO^+ are similar in the two models, but for DCN/HCN and $HDCO/H_2CO$ there is a drop in deuteration with the higher disk mass. DCN and HCN exist in a layer above the midplane in both models, with the Model 2 layer being at slightly higher z due to the increase in optical depth of this model. In both models, the abundance of DCN is mainly dependent on the ratio of D atoms which react with HNC to form DCN, and H atoms which destroy DCN forming HCN. The ratio of atomic D/H is higher in Model 1 than Model 2, leading to a higher DCN/HCN ratio.

3.5. Comparison with Previous Inner Disk Models

Markwick et al. (2002) use a similar, but undeuterated, chemical network to model the chemistry within 10 AU of a protostar. However there are major differences between our disk model and theirs which result in very different temperature structures and hence different calculated abundances. Although our Model 1 and that used by Markwick et al. have similar grain temperatures in the midplane at 10 AU, their model has a more rapid increase in midplane temperature as the radius decreases. They also find a vertical temperature inversion at all radii (< 10 AU) so that the surface layers are cooler than the midplane. The relative surface and midplane temperatures are controlled in part by the surface density of the disk—the higher the surface density, the thicker the disk and the warmer the midplane is relative to the surface layers. The Markwick et al. disk has a mass accretion rate that is 10× higher than ours, leading to a higher surface density and hence a colder surface temperature.

The grain temperature is very important since it governs the location at which molecules can desorb. Markwick et al. find that at 10 AU almost all the molecules are accreted onto grains in the surface layer. Because of our higher grain temperature in this region, we find most molecules are in the gas phase, with only water and its isotopologues remaining as ice. We also find that grain mantles persist at smaller radii compared to Markwick, again because of the difference in temperature distribution assumed.

More recently, the chemistry in the disk within 3 AU of the star has been studied by Agúndez et al. (2008). These authors concentrated on the warm, UV irradiated, surface regions and found that photodissociation of CO provided a pool of carbon atoms that leads to the formation of simple organics such as C_2H_2, HCN, and CH_4. The formation of C_2H_2 depends on the reaction of H_2 with either C_2 or C_2H—reactions that are not generally included in astrochemical models since they have activation barriers of ∼ 1400 K. However, in the warm inner disk the gas temperatures are high enough for them to make a significant contribution to the carbon chemistry. These authors find good agreement with observations and their results (apart from C_2H_2) are in broad agreement with those presented here.

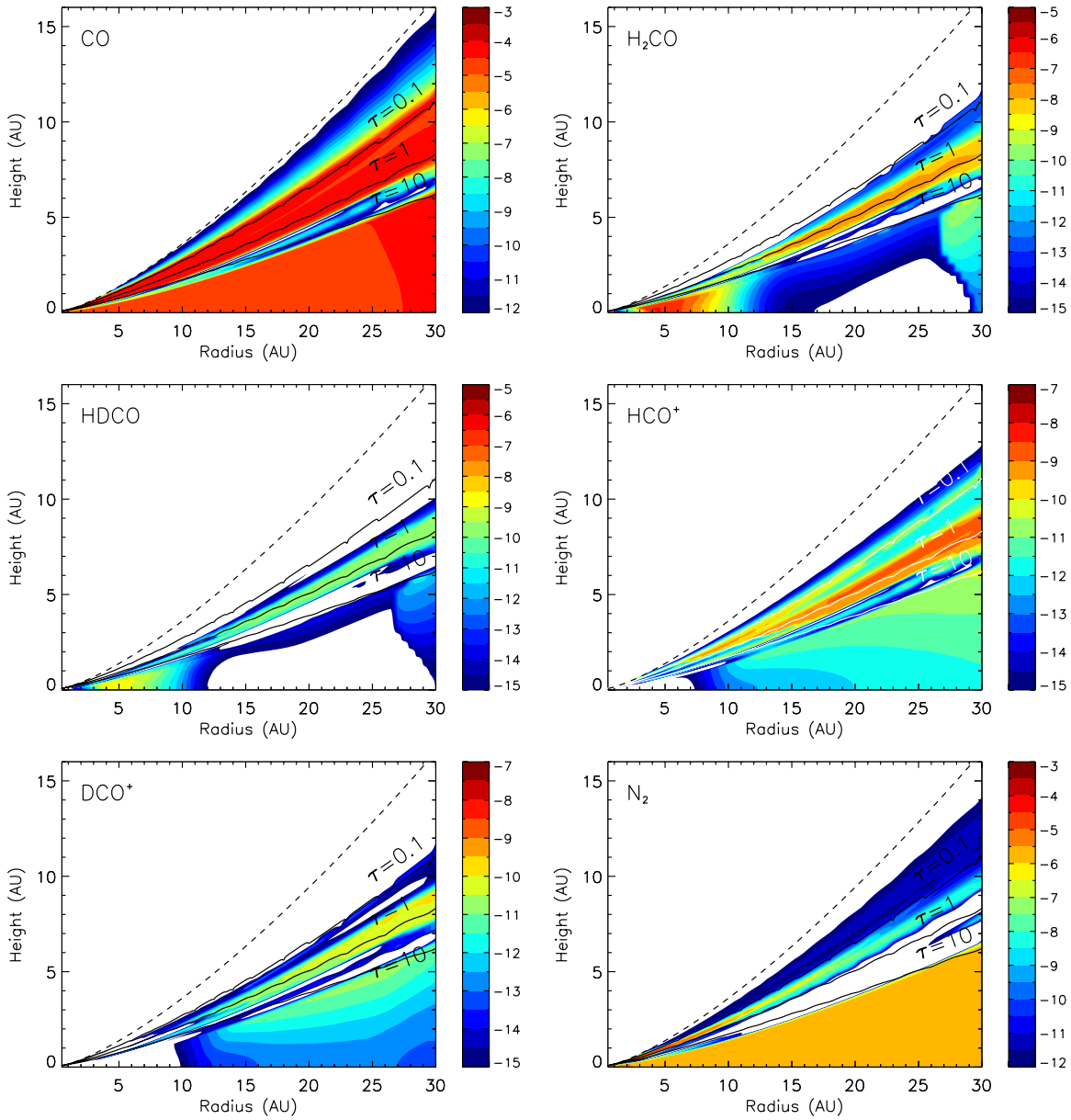

Figure 9. Fractional abundances in the inner disk for Model 2 ($\alpha = 0.025$). The first few figures, from CO to CN, show those molecules which are present throughout the disk; the later ones show those molecules which are only present in the gas phase in the inner 10 AU.

(A color version of this figure is available in the online journal.)

Deuterium chemistry has previously been studied in the inner disk by Aikawa & Herbst (1999) who followed the evolution of material into a radius of 30 AU. Their model differs from ours in several ways. They include a description of the effects of collapse on the input abundances. Although they include gas–grain interactions (freezeout and thermal desorption) they do not consider the effects of reactions on the grain surface (except for the formation of H_2 and for recombination of ions and electrons). This leads to a number of important differences between their conclusions and ours. Aikawa & Herbst find that gas-phase chemistry is important for determining the deuteration of some molecules. Most notably this includes the DCN/HCN ratio observed in comets. They find that DCN and HCN are formed by CHD + N $\longrightarrow$ DCN + C and CH_2 + N $\longrightarrow$ HCN + C, respectively. The derived ratio can be affected by both the cosmic ray ionization rate (lowering ζ_{CR} results in a lower D/H ratio) and by whether or not HCO^+ recombines dissociatively with electrons on grain surfaces. In contrast, we find that to a large extent the DCN/HCN ratio calculated in ices at the comet formation radius in our disk is driven by what happened in the molecular cloud, where grain surface chemistry plays an important role in determining the deuteration.

We know from observations that the amount of water ice seen in molecular clouds can only be produced by grain chemistry. This alone demonstrates the importance of considering grain chemistry in models, but the mechanism for including it is still a matter for debate. Another issue that remains unresolved is the nature of non-thermal desorption processes that prevent the complete removal of molecules from the gas in regions where thermal desorption is inefficient. Other observations of star-forming regions (Parise et al. 2002; Loinard et al. 2002; Bacmann et al. 2003) also indicate that grain chemistry is important in the formation of molecules such as deuterated formaldehyde and methanol, and hence cannot be ignored

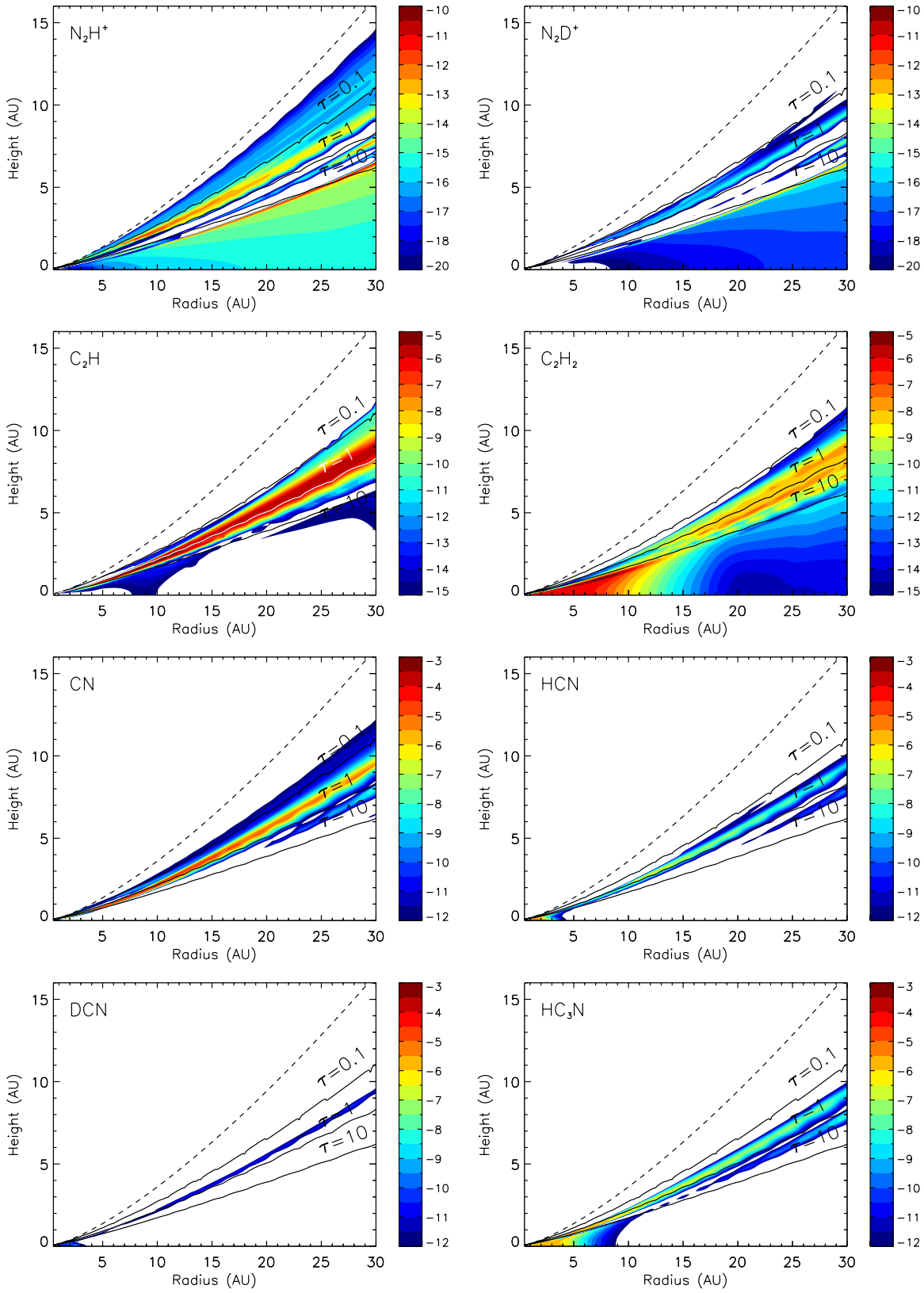

Figure 9. (Continued)

when modeling deuteration effects. Equally our model falls short in not considering the collapse phase and the effects on the chemistry of the incorporation of cloud material into the protostellar disk. Neither our model nor that of Aikawa & Herbst (1999) provides a complete picture of the chemical history of disks.

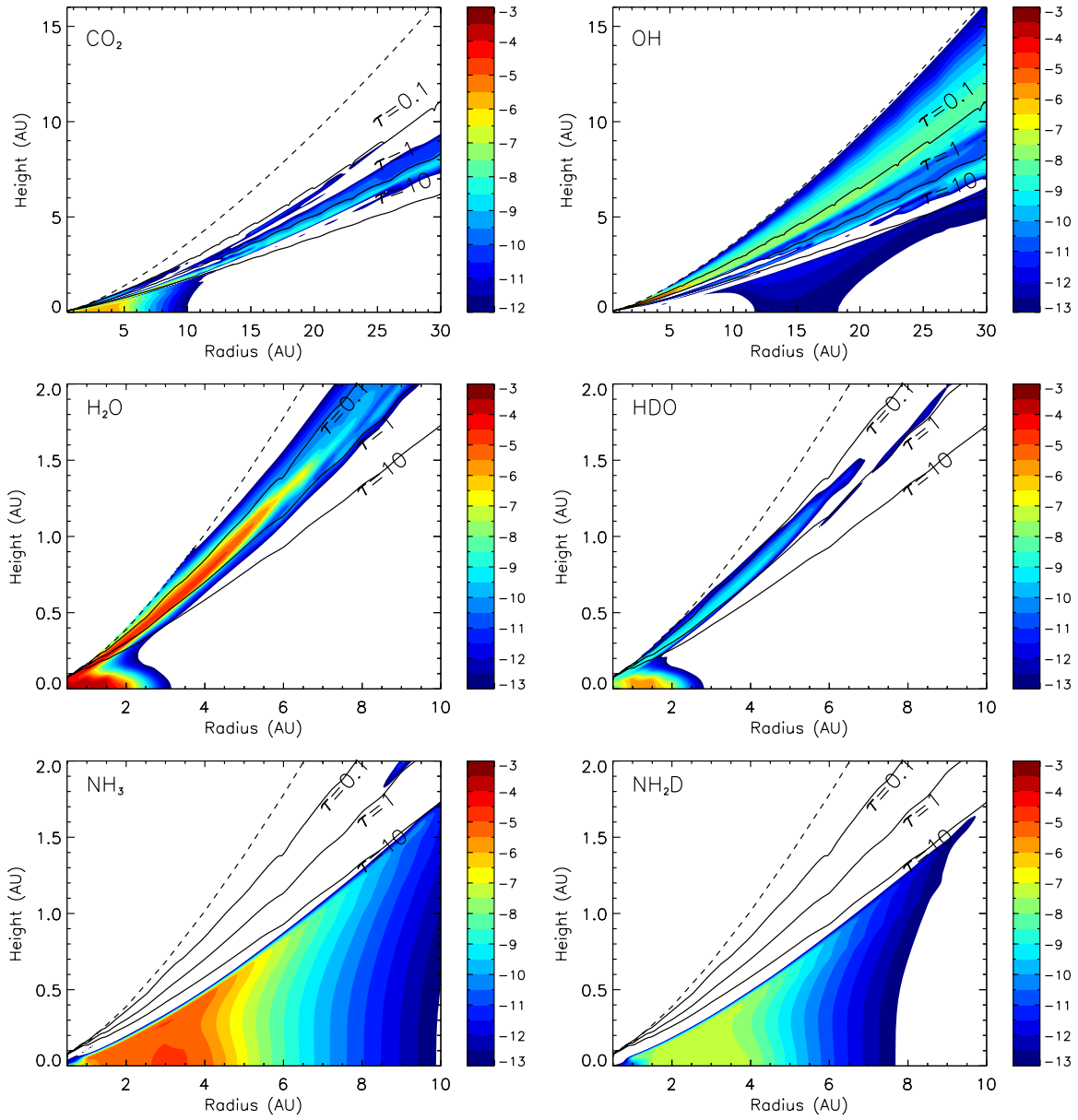

Figure 9. (Continued)

4. COMPARISON TO OBSERVATIONS

4.1. Cometary Ices

The comets we see today are the remains of icy planetesimals that formed early in the history of the solar system. Since their formation they have been kept mainly at cold temperatures which restrict further chemical evolution. Consequently, their chemical make up reflects to first order, the composition of the protostellar disk at their time of formation. Simple species such as H_2O, CO, CO_2, HCN, CH_3OH, H_2CO have been observed in the comae of many comets, but D/H ratios have been measured in only four comets—Halley (HDO/H_2O), Hyakutake (HDO/H_2O), Hale-Bopp (DCN/HCN, HDO/H_2O), and C/2002 T7 (LINEAR). These are all long-period comets, and so formed inside of the Trans-Neptunian region, after which their orbits were perturbed by interaction with the giant planets and they were ejected outward toward the Oort cloud. The chemical composition of the comets should reflect the temperature, density, and ionization state of the region in which they formed. Measurements of the D/H ratios of cometary ices could also be used to constrain the degree of processing of the interstellar ices incorporated into the protosolar disk, and place limits on the amount of radial mixing experienced by material in the disk.

The observed molecular deuteration is similar for all four comets. In Hale-Bopp, $DCN/HCN = 2.3 \times 10^{-3}$ (Meier et al. 1998). $(D/H)_{H_2O}$ is measured as 3.3×10^{-4} in Hale-Bopp (Meier et al. 1998), 2.9×10^{-4} in Hyakutake (Bockelee-Morvan et al. 1998) and $\sim 3.1 \times 10^{-4}$ (Eberhardt et al. 1995; Balsiger et al. 1995) in Comet/P Halley. In C/2002 T7 (LINEAR) $(D/H)_{H_2O}$ is 2.5×10^{-4} (Hutsemékers et al. 2008). (These measurements correspond to $x(HDO)/x(H_2O)$ ratios of 6.6×10^{-4}, 5.8×10^{-4}, 6.2×10^{-4}, and 5.0×10^{-4} for Hale-Bopp, Hyakutake, Halley, and C/2002 T7 (LINEAR), respectively.)

Table 4 gives the deuteration of some molecules at different radii in the mid plane of the disk. Figure 11 shows the variation in the $x(DCN)/x(HCN)$ and $x(HDO)/x(H_2O)$ ratios in the ice

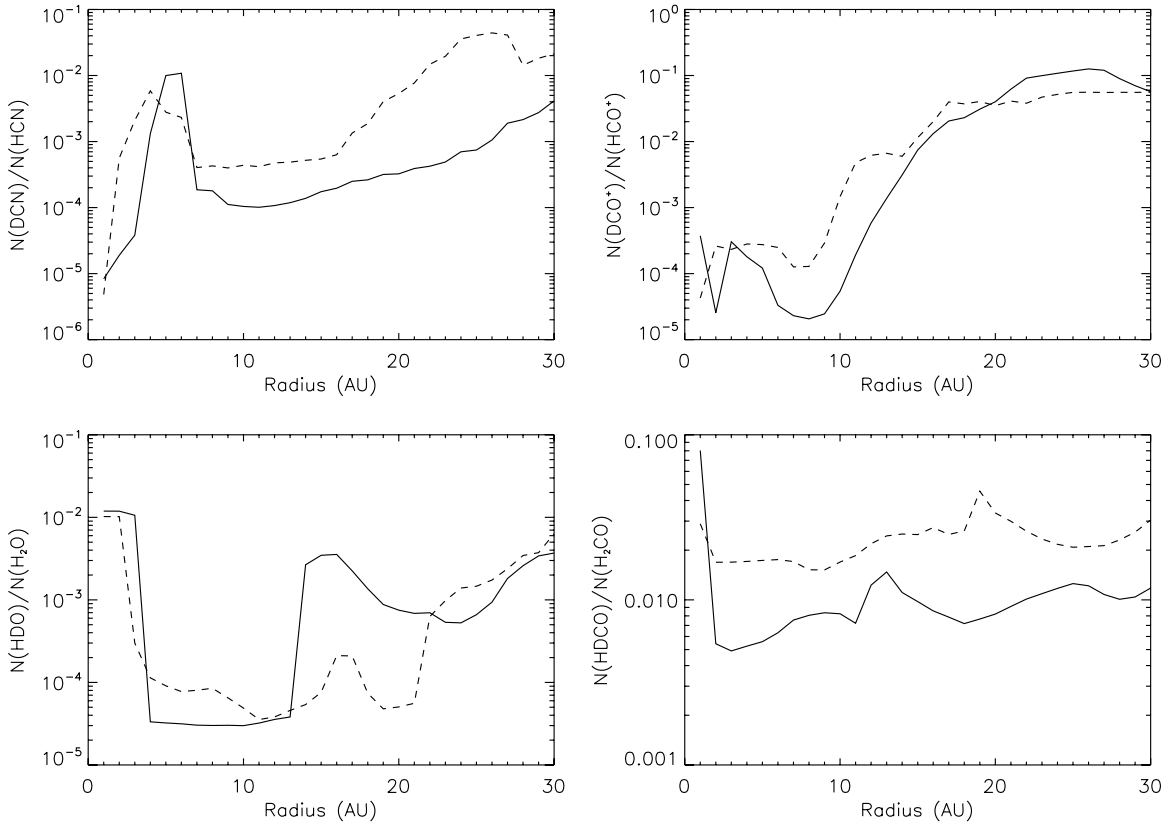

Figure 10. Radial variation of column density deuteration (i.e., N(XD)/N(XH)) for Models 1 (dashed line) and 2 (solid line).

Table 4
The Molecular D/H Ratios in the Midplane for Model 1

Molecule	Input	25 AU	10 AU	5 AU	1 AU
D/H	2.00 (−2)	5.25 (−3)	6.70 (−5)	5.50 (−3)	5.50 (−6)
DCO^+/HCO^+	9.00 (−2)	1.89 (−2)	2.30 (−2)	...	...
CH_2D/CH_3^+	1.10 (−1)	...	...	...	...
H_2D^+/H_3^+	2.00 (−1)	...	...	...	...
$HDCO/H_2CO$	7.00 (−2)	1.69 (−2)	1.07 (−2)	1.60 (−2)	...
HDO/H_2O	1.00 (−1)	...	...	...	1.00 (−2)
D_2O/H_2O	1.00 (−3)	...	...	...	1.06 (−4)
DCN/HCN	3.20 (−2)	...	...	...	5.53 (−6)
NH_2D/NH_3	3.10 (−2)	...	...	4.09 (−3)	4.50 (−3)
HDO:gr/H_2O:gr	9.00 (−3)	9.34 (−3)	9.50 (−3)	9.60 (−3)	1.07 (−2)
DCN:gr/HCN:gr	9.00 (−3)	3.00 (−2)	2.96 (−2)	2.99 (−3)	...
HDCO:gr/H_2CO:gr	4.80 (−2)	2.96 (−2)	1.54 (−2)	2.17 (−3)	...
NH_2D:gr/NH_3:gr	5.13 (−3)	5.34 (−3)	5.26 (−3)	5.26 (−3)	...

Notes. ... indicates that the molecular fractional abundances are very low ($< 10^{-15}$). X:gr indicates a grain mantle species.

mantles over the radius range from 0.5 to 10 AU. Our model shows very little variation in the ratios in the midplane in this region. The x(HDO)/x(H_2O) ratio is set in the molecular cloud phase and very little processing of the water ice occurs in the disk. Hence in the midplane, the x(HDO)/x(H_2O) ratio in ices has a constant value of 0.022 from 30 to 2 AU. DCN/HCN shows some slight variation but the value is still roughly 0.018 from 5 to 10 AU. For both molecules, the model deuteration ratios are much higher than observed. The model DCN/HCN is approximately 8 times higher than observed, and the HDO/H_2O ratio is 33–44 times higher than observed. Hence, although comets have to contain ices accumulated at low temperatures they must also include some ices that were formed in a higher temperature phase.

There are several possible explanations for the discrepancy between our model and the observations. Since the disk chemistry does not change, the HDO/H_2O ratio from the value set in the molecular cloud it may be that the problem lies in our molecular cloud model, and that HDO ice is formed too efficiently. In our cloud model, the ratio of HDO/H_2O in the ice is 0.9%, compared to an upper limit of $\sim$ 0.5%–2% toward low-mass protostars (Parise et al. 2003). This upper limit is much less than the deuteration ratios seen in methanol and formaldehyde which are also expected to form on grain surfaces. If all three

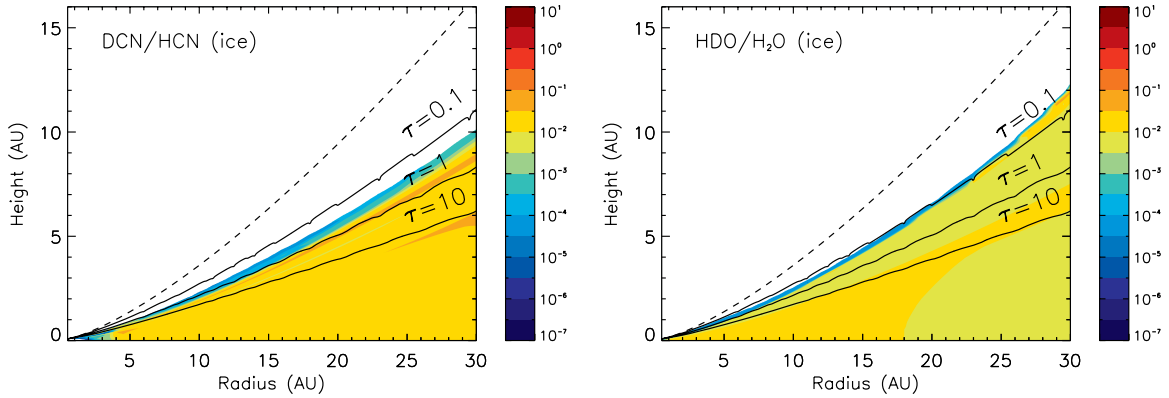

Figure 11. Deuteration of HCN and H_2O ices in Model 2.
(A color version of this figure is available in the online journal.)

molecules form at the same time then their D/H ratios should be similar and should reflect the gas-phase atomic D/H ratio at the time of formation. Observations of methanol and formaldehyde in low-mass star formation regions find much higher D/H ratios that the upper limit derived for HDO/H_2O ice, suggesting that there are still unresolved issues in our understanding of the formation of these molecules.

Another possibility is that the ices are removed from the grains during infall through the accretion shock at the surface of the disk. Models suggest that most of the water ice on infalling grains can be removed within 30 AU of a solar type star (e.g., Lunine et al. 1991; Neufeld & Hollenbach 1994). Recent Spitzer observations (Watson et al. 2007) have found water vapor emission in a Class 0 object (NGC 1333-IRAS 4B), which has been attributed to emission from a surface accretion shock. Water would therefore enter the disk as vapor rather than as ice. This could affect the D/H ratio of the ices that reform in the disk, since water formed in the warm post-shock region would have a lower D/H ratio than water formed in the cold molecular cloud, and this ratio would be transferred to the ices when the molecules were redeposited. However, it is unclear how widespread or long-lived this phenomenon is since water emission was detected in only one object out of a sample of 30.

Although vertically averaged hydrodynamical disk models find that material is advected radially inward, e.g., Pringle (1981); Lin & Papaloizou (1985), with outward flow occurring only in the cold outer regions of the disk, more complex models have shown that large-scale meridional flow patterns develop in disks, e.g., Urpin (1984); Kley & Lin (1992); Rozyczka et al. (1994); Regev & Gitelman (2002); Tscharnuter & Gail (2007). In these models, material flows inward at the surface and outward in the midplane, leading to a mixing of warm and cold material. Observational evidence of the importance of mixing in disks comes from comets. Silicates are thought to have undergone significant high-temperature processing, which converted amorphous silicates into the crystalline form, before they were incorporated into comet nuclei (Hanner 1999). One way to do this would be by radial mixing where the silicates were heated to high temperatures in the inner disk before being mixed outward to the comet formation region. Additional evidence of mixing in the history of comets has been seen in the STARDUST samples (Brownlee et al. 2006; Zolensky et al. 2006). If grains can be mixed, then gases could be too, and this would have the effect of changing the deuteration ratios by bringing together molecules formed in the cold outer disk or in the molecular cloud with those formed in warmer regions of the disk. Overall, mixing could be expected to reduce the D/H ratios seen in cometary ices.

Diffusion has been included in models of the deuterium chemistry in the midplane of disks by Drouart et al. (1999) and Mousis et al. (2000). Drouart et al. (1999) assume that the water is initially gaseous with $(D/H)_{H_2O} = (D/H)_{H_2}$ and they follow the evolution of $(D/H)_{H_2O}$ over time in a model that includes turbulent diffusion. Mousis et al. (2000) take a similar approach and modeled the DCN/HCN ratio. These authors concluded that cometary ices condense in the nebula, rather than being retained during the disk and star formation, and are composed of material that is partially reprocessed in the disk. Horner et al. (2007) also found a relationship between the D/H ratios in ices and the distance from the Sun at which they condense.

Our model is, therefore, probably too simplistic in its assumptions and further work is required to study how the accretion shock alters the D/H ratios and the survivability of the ices in the star formation process, and to consider the effects of mixing. Ilgner et al. (2004), Semenov et al. (2006), and Willacy et al. (2006) have all shown that mixing in the vertical direction can greatly affect the abundances in the disk, but isotopes have not yet been studied with these models. Also, as shown by Drouart et al. (1999), Mousis et al. (2000), and Horner et al. (2007), radial mixing alters D/H ratios in ices, bringing cold material into the inner disk where it can desorb and returning material to the colder regions where it can reaccrete. Both radial and vertical diffusion alter the molecular D/H ratios by combining material formed under different temperature regimes.

4.2. Gas-phase Observations of Extrasolar Disks

Our basic model (excluding isotopes) is the same as used in Woods & Willacy (2009) who considered the chemistry of carbon isotopes. That paper includes a comparison of the result to recent infrared observations of the inner regions of protostellar disks. Here we merely summarize our findings for completeness, but the reader is referred to Woods & Willacy (2009) for more details.

Several molecules, e.g., CO, C_2H_2, HCN, OH, H_2O, and CO_2 have been observed in AA Tau (Carr & Najita 2008), DR Tau and AS 205 A (Salyk et al. 2008), GV Tau (Gibb et al. 2004, 2007), and IRS 46 (Lahuis et al. 2006). The derived rotational temperatures suggest that the molecular emission comes from a region above the midplane. In our models, these temperatures are reached in the region where thermal desorption is efficient, and the gas and grain temperatures are decoupled. We find that in Model 1, CO, H_2O, and OH have peak abundances in

Table 5
The Observed Column Densities in the Inner Regions of Protostellar Disks

Molecule	Column Density (10^{16} cm^{-2})					
	GV Tau[1]	IRS46[2]	AA Tau[3]	AS 205A[4]	DR Tau[4]	Model 1
H_2O	...	...	65.0	60.0	80.0	1280.0
OH	...	...	8.1	20.0	20.0	23.0
HCN	3.7	5.0	6.5	...	...	4.4
C_2H_2	7.3	3.0	0.8	...	...	9.0 (−8)
CO_2	...	10.0	0.2	...	...	13.0
CO	590.0	200.0	49.0	60.0	70.0	1600.0

Note. The values for Model 1 are calculated at 1 AU for the surface layers of the disk where $T_{gas} > 150$ K.
References. (1) Gibb et al. 2007; (2) Lahuis et al. 2006; (3) Carr & Najita 2008; (4) Salyk et al. 2008.

Table 6
Calculated Vertical Column Densities from Midplane to the Disk Surface for Some Gas-Phase Species in Models 1 and 2

Molecule	Model 1 ($\alpha = 0.01$)			Model 2 ($\alpha = 0.025$)		
	1 AU	5 AU	10 AU	1 AU	5 AU	10 AU
H_2	1.6 (25)	2.4 (24)	2.3 (24)	4.9 (25)	1.9 (25)	9.2 (24)
CO	1.1 (21)	3.8 (20)	3.6 (20)	1.9 (21)	1.9 (21)	6.0 (20)
CO_2	3.5 (19)	1.2 (18)	7.0 (14)	7.3 (19)	1.7 (19)	6.8 (13)
H_2O	4.1 (21)	8.2 (16)	2.5 (16)	1.4 (22)	1.4 (17)	7.1 (15)
HDO	4.2 (19)	6.4 (12)	8.7 (11)	1.7 (20)	8.7 (12)	2.6 (11)
OH	2.4 (17)	7.6 (16)	6.8 (16)	1.2 (17)	1.1 (17)	8.3 (16)
HCN	1.1 (20)	6.6 (14)	4.2 (14)	4.1 (20)	1.8 (14)	3.6 (14)
DCN	5.0 (14)	2.4 (11)	4.3 (10)	2.6 (15)	1.4 (10)	2.6 (10)
CN	1.5 (18)	2.2 (17)	8.6 (16)	3.4 (18)	1.9 (17)	8.3 (16)
C_2H_2	2.0 (19)	6.0 (18)	3.6 (16)	3.3 (19)	2.2 (19)	2.5 (17)
CH_4	6.5 (18)	2.3 (18)	4.5 (18)	2.8 (18)	4.8 (18)	9.5 (17)

regions of the disk with similar temperatures to the observed rotation temperatures for these molecules. The surface peak of CO_2 also coincides with the observed rotation temperature, although the peak abundance of this molecule is closer to the midplane. For C_2H_2 the observations lie above the modeled distribution, and for HCN they are at the upper edge of the model.

We can also compare our results with the column densities observed (Table 5). The calculated column densities at 1 AU for several molecules are given in Table 6 and are much higher than observed, but these values are calculated from the disk midplane to its surface and therefore include material that is much colder than observed. If we instead calculate the column densities only in the upper regions of the disk where the gas temperature is warmer than 150 K, the agreement is better. The calculated column densities are $N(\mathrm{HCN}) = 4.4 \times 10^{16}$ cm^{-2}, $N(\mathrm{CO}) = 1.6 \times 10^{19}$ cm^{-2}, and $N(\mathrm{CO_2}) = 1.3 \times 10^{17}$ cm^{-2} for Model 1. $N(\mathrm{C_2H_2})$ is far too low (9×10^{8} cm^{-2}). This low abundance may be due to the exclusion of reactions involving H_2 with C_2 or C_2H that were found to be important in the formation of C_2H_2 in disks by Agúndez et al. (2008) but are not included in our reaction scheme. The calculated $N(H_2O)$ is also too high compared to observations, but N(OH) gives good agreement with the abundances measured in DR Tau and AS 205A Salyk et al. (2008).

A further test of the models is to compare the CH_4/CO ratio. Gibb et al. (2007) found an upper limit of 0.0035, similar to the upper limit Gibb et al. (2004) found for this ratio in HL Tau ($<$ 0.005). The calculated ratio at 1 AU of 0.006 is consistent with both these observational measurements.

Table 7
The Calculated Values of $N(\mathrm{DCO^+})$, $N(\mathrm{HCO^+})$, and $\mathrm{DCO^+/HCO^+}$

	30 AU	50 AU	100 AU	150 AU
$N(\mathrm{DCO^+})$	1.9 (12)	1.5 (12)	6.6 (12)	2.3 (12)
$N(\mathrm{HCO^+})$	3.3 (13)	1.2 (13)	3.9 (12)	2.8 (12)
$\mathrm{DCO^+/HCO^+}$	0.05	0.125	1.7	0.8

Note. The Data for $R > 30$ AU are taken from Willacy (2007).

Qi et al. (2008) observed deuterated molecules in TW Hya and found a gradient in the $\mathrm{DCO^+/HCO^+}$ ratio. The ratio increases from 0.01 at 30 AU to 0.1 at $\sim$ 70 AU. There is a steep falloff in $N(\mathrm{DCO^+})$ at $R > 90$ AU. Our current model only extends out to 35 AU but when we consider it together with our outer disk model (Willacy 2007) we can see if the same trend shows up in the chemical modeling data. Table 7 shows the model column densities for $\mathrm{DCO^+}$ and $\mathrm{HCO^+}$, as well as their ratio for radii between 30 and 150 AU. Although we do not find the same steep falloff in $N(\mathrm{DCO^+})$ at $R > 90$ AU, we do see a similar increase in $\mathrm{DCO^+/HCO^+}$ from 30 to 100 AU followed by a fall at larger radii. However, our D/H ratio at 100 AU is $\sim 10 \times$ larger than inferred from the observational data.

5. CONCLUSIONS

We have presented the results of calculations of the chemical abundances in the inner regions of protostellar disks including deuterium chemistry. We find that for many molecules the deuteration is set by cold temperature chemistry in the parent molecular cloud, and that the chemistry in the disk itself has little effect. In particular, the calculated D/H ratios in ices in the region of cometary formation are found to be high relative to the (limited) cometary observations. This suggests that our model is not complete, and additional processing of ices is required after the molecular cloud stage, beyond the chemistry included in our models here. Our carbon isotope modeling leads to a similar conclusion (Woods & Willacy 2009). The processing could be achieved in the accretion shock, and/or by mixing in the disk, both of which could lead to lower D/H ratios. Additional work is required to fully understand the process by which interstellar grains and ices are incorporated into planets and other planetary bodies.

When a comparison is made with the observations of external disks (Carr & Najita 2008; Gibb et al. 2007, 2004) good agreement is found between the location of the molecules in our disks and that derived from the observations. The molecular emission comes from a region above the midplane, where thermal desorption is efficient.

We find major differences in the results of our calculations and those of other models, mainly as a consequence of either the physical disk model assumed, or because of the chemical processes included. We find that the disk chemistry has less effect on D/H ratios than Aikawa & Herbst (1999) because we allow chemistry to occur on the surfaces of dust grains and hence gas-phase chemistry is less important in determining deuteration. The temperature structure in our models is very different to that assumed by Markwick et al. (2002), so that, despite using similar chemical networks, we get very different abundance distributions in the inner 10 AU of the disk. This highlights the effect that the disk structure can have on the molecular distributions in disks. As observations improve in resolution, for example, with the advent of ALMA this may enable the differences between models to be used to distinguish among them observationally.

This research was conducted at the Jet Propulsion Laboratory, California Institute of Technology under contract with the National Aeronautics and Space Administration. Partial support was provided to K.W. by a grant from the NASA TPF Foundation Science program. A portion of this research was carried out while P.M.W. was supported by an appointment to the NASA Postdoctoral Program at JPL, administered by ORAU through a contract with NASA. We also wish to acknowledge the helpful comments of Bockelée-Morvan concerning the measurements of the D/H ratio in cometary water.

REFERENCES

Agúndez, M., Cernicharo, J., & Goicoechea, J. R. 2008, A&A, 483, 831
Aikawa, Y., & Herbst, E. 1999, A&A, 351, 223
Aikawa, Y., van Zadelhoff, G. J., van Dishoeck, E. F., & Herbst, E. 2002, A&A, 386, 622
Allen, M., & Robinson, G. W. 1977, ApJ, 212, 396
Bacmann, A., Lefloch, B., Ceccarelli, C., Steinacker, J., Castets, A., & Loinard, L. 2003, ApJ, 585, 55
Balbus, S. A., & Hawley, J. F. 1991, ApJ, 376, 214
Balbus, S. A., Hawley, J. F., & Stone, J. M. 1996, ApJ, 467, 76
Balsiger, H., Altwegg, K., & Geiss, J. 1995, J. Geophys. Res., 100, 5827
Barsuhn, J. 1977, ApJS, 28, 453
Ben Jaffel, L., Vidal-Madjar, A., Gladstone, G. R., McConnell, J. C., Emerich, C., Prange, R., & Clarke, J. T. 1998, in ASP Conf. Ser. 143, The Scientific Impact of the Goddard High Resolution Spectrograph, ed. J. C. Brandt, T. B. Ake, & C. C. Petersen (San Francisco, CA: ASP), 366
Bergin, E., Calvet, N., d'Alessio, P., & Herczeg, G. J. 2003, ApJ, 591, 159
Bergin, E. A., Aikawa, Y., Blake, G. A., & van Dishoeck, E. F. 2007, in Protostars and Planets V, ed. B. Reipurth, D. Jewitt, & K. Keil (Tucson, AZ: Univ. Arizona Press), 751
Bézard, B., Encrenaz, T., Feuchtgruber, H., Lellouch, E., de Graauw, T., Griffin, M., & Atreya, S. K. 1997, BAAS, 29, 993
Blaes, O. M., & Balbus, S. A. 1994, ApJ, 421, 163
Bockelee-Morvan, D., et al. 1998, Icarus, 133, 147
Brown, P. D., & Millar, T. J. 1989, MNRAS, 240, 25
Brownlee, D., et al. 2006, Science, 314, 1711
Carr, J. S., & Najita, J. R. 2008, Science, 319, 1504
Caselli, P., Stantcheva, T., Shalabiea, O., Shematovich, V. I., & Herbst, E. 2002, Planet. Space Sci., 50, 1257
Cazaux, S., & Tielens, A. G. G. M. 2002, ApJ, 575, 29
Cazaux, S., & Tielens, A. G. G. M. 2004, ApJ, 604, 222
Ceccarelli, C., & Dominik, C. 2005, A&A, 440, 583
Ceccarelli, C., Dominik, C., Caux, E., Lefloch, B., & Caselli, P. 2005, ApJ, 631, 81
Ceccarelli, C., Dominik, C., Lefloch, B., Caselli, P., & Caux, E. 2004, ApJ, 607, 51
Charnley, S. B., Tielens, A. G. G. M., & Rodgers, S. D. 1997, ApJ, 482, 203
d'Alessio, P., Calvet, N., & Hartmann, L. 2001, ApJ, 553, 321
d'Alessio, P., Calvet, N., Hartmann, L., Lizano, S., & Canto, L. 1999, ApJ, 527, 893
Dominik, C., Ceccarelli, C., Hollenbach, D., & Kaufman, M. 2005, ApJ, 635, L85
Draine, B. T., & Lee, H. M. 1984, ApJ, 285, 89
Drouart, A., Dubrulle, B., Gautier, D., & Robert, F. 1999, Icarus, 140, 129
Dubrulle, B. 1993, Icarus, 106, 59
Dubrulle, B., Marié, L., Normand, C., Richard, D., Hersant, F., & Zahn, J.-P. 2005, A&A, 429, 1
Dutrey, A., Guilloteau, S., & Guélin, M. 1997, Astron. Astrophys. Lett., 317, 5
Eberhardt, P., Reber, M., Krankowsky, D., & Hodges, R. R. 1995, A&A, 302, 301
Encrenaz, T., Drossart, P., Feuchtgruber, H., Lellouch, E., Bézard, B., Fouchet, T., & Atreya, S. K. 1999, Planet. Space Sci., 47, 1225
Feuchtgruber, H., Lellouch, E., Bézard, B., Encrenaz, T., de Graauw, T., & Davis, G. R. 1999, A&A, 341, L17
Fraser, H. J., Collings, M. P., McCoustra, M. R. S., & Williams, D. A. 2001, MNRAS, 327, 1165
Fromang, S., Terquem, C., & Balbus, S. A. 2002, MNRAS, 329, 18
Gammie, C. F. 1996, ApJ, 457, 355
Geppert, W. D., et al. 2004, ApJ, 609, 459
Gibb, E. L., Rettig, T., Brittain, S., Haywood, R., Simon, T., & Kulesa, C. 2004, ApJ, 610, 113
Gibb, E. L., Van Brunt, K. A., Brittain, S. D., & Rettig, T. W. 2007, ApJ, 660, 1572
Gorti, U., & Hollenbach, D. 2004, ApJ, 613, 424
Guilloteau, S., & Dutrey, A. 1998, A&A, 369, 467
Guilloteau, S., Piétu, V., Dutrey, A., & Guélin, M. 2006, A&A, 448, 5
Hanner, M. 1999, Space Sci. Rev., 90, 99
Hasegawa, T. I., & Herbst, E. 1993, MNRAS, 261, 83
Hasegawa, T. I., Herbst, E., & Leung, C. M. 1992, ApJS, 82, 167
Hawley, J. F., & Balbus, S. A. 1991, ApJ, 376, 223
Hawley, J. F., Gammie, C. F., & Balbus, S. A. 1996, ApJ, 464, 690
Hayashi, C. 1981, Prog. Theor. Phys. Suppl., 70, 35
Horner, J., Mousis, O., & Hersant, F. 2007, Earth Moon Planets, 100, 43
Hutsemékers, D., Manfroid, J., Jehin, E., Zucconi, J.-M., & Arpigny, C. 2008, A&A, 490, 31
Ilgner, M., Henning, T., Markwick, A. J., & Millar, T. J. 2004, A&A, 415, 643
Ilgner, M., & Nelson, R. P. 2006a, A&A, 445, 205
Ilgner, M., & Nelson, R. P. 2006b, A&A, 445, 223
Ilgner, M., & Nelson, R. P. 2006c, A&A, 455, 731
Inutsuka, S.-i., & Sano, T. 2005, ApJ, 628, 155
Kamp, I., & Dullemond, C.-P. 2004, ApJ, 615, 991
Kastner, J. H., Zuckerman, B., Weintraub, D. A., & Forveille, T. 1997, Science, 277, 67
Klahr, H. H. 2004, ApJ, 606, 1070
Klahr, H. H., & Bodenheimer, P. 2003, ApJ, 582, 869
Kley, W., & Lin, D. N. C. 1992, ApJ, 397, 600
Lahuis, F., et al. 2006, ApJ, 636, 145
Lee, H.-H., Herbst, E., Pineau des Forets, G., Roueff, E., & Le Bourlot, J. 1996, A&A, 311, 690
Lellouch, E., Bézard, B., Fouchet, T., Feuchtgruber, H., Encrenaz, T., & de Graauw, T. 2001, A&A, 370, 610
Li, H., Finn, J. M., Lovelace, R. V. E., & Colgate, S. A. 2000, ApJ, 553, 1023
Lin, D. N. C., & Papaloizou, J. 1980, MNRAS, 191, 37
Lin, D. N. C., & Papaloizou, J. 1985, in Protostars and Planets II, ed. D. C. Black & M. S. Matthews (Tucson, AZ: Univ. Arizona Press), 981
Linsky, J. L., et al. 2006, ApJ, 647, 1106
Loinard, L., et al. 2002, Planet. Space Sci., 50, 1205
Lunine, J. I., Engel, S., Rizk, B., & Horanyi, M. 1991, Icarus, 94, 333
Mahaffy, P. R., Donahue, T. M., Atreya, S. K., Owen, T. C., & Niemann, H. B. 1998, Space Sci. Rev., 84, 251
Markwick, A. J., Ilgner, M., Millar, T. J., & Henning, T. 2002, A&A, 385, 632
Matsumura, S., & Pudritz, R. E. 2003, ApJ, 598, 645
Matsumura, S., Pudritz, R. E., & Thommes, E. W. 2007, ApJ, 660, 1609
Meier, R., et al. 1998, Science, 279, 1707
Messenger, S. 2000, Nature, 404, 968
Messenger, S., Stadermann, F. J., Floss, C., Nittler, L. R., & Mukhopadhyay, S. 2003, Space Sci. Rev., 106, 155
Millar, T. J., Bennett, A., & Herbst, E. 1989, ApJ, 340, 906
Millar, T. J., Farquhar, P. R. A., & Willacy, K. 1998, A&AS, 121, 139
Molek, C. D., McLain, J. L., Poterya, V., & Adams, N. G. 2007, J. Phys. Chem, 111, 6760
Morfill, G. E., & Völk, H. J. 1984, ApJ, 287, 371
Mousis, O., Gautier, D., Bockelée-Morvan, D., Robert, F., Dubrulle, B., & Drouart, A. 2000, Icarus, 148, 513
Neufeld, D. A., & Hollenbach, D. J. 1994, ApJ, 428, 170
Öberg, K. I., van Broekhuizen, F., Fraser, H. J., Bisschop, S. E., van Dishoeck, E. F., & Schlemmer, S. 2005, ApJ, 621, L33
Orton, G. S., Lacy, J. H., Achtermann, J. M., Parmar, P., & Blass, W. E. 1992, Icarus, 100, 541

Owen, T., Lutz, B. L., & de Bergh, C. 1986, Nature, 320, 244
Parise, B., Simon, T., Caux, E., Dartois, E., Ceccarelli, C., Rayner, J., & Tielens, A. G. G. M. 2003, A&A, 410, 897
Parise, B., et al. 2002, A&A, 393, 49
Pizzarello, S., & Huang, Y. 2005, Geochim. Cosmochim. Acta, 69, 599
Preibisch, T., Ossenkopf, V., Yorke, H. W., & Henning, T. 1993, A&A, 279, 577
Pringle, J. E. 1981, ARA&A, 19, 137
Qi, C., Wilner, D. J., Aikawa, Y., Blake, G. A., & Hogerheijde, M. R. 2008, ApJ, 681, 1396
Regev, O., & Gitelman, L. 2002, A&A, 396, 623
Remusat, L., Palhol, F., Robert, F., Derenne, S., & France-Lanord, C. 2006, Earth Planet. Sci. Lett., 243, 15
Richling, S., & Yorke, H. W. 2000, ApJ, 539, 258
Robert, F., Gautier, D., & Dubrulle, B. 2000, Space Sci. Rev., 92, 201
Roberts, H., Herbst, E., & Millar, T. J. 2002, MNRAS, 336, 283
Roberts, H., Herbst, E., & Millar, T. J. 2003, ApJ, 591, 41
Roberts, H., Herbst, E., & Millar, T. J. 2004, A&A, 424, 905
Roberts, H., & Millar, T. J. 2000, A&A, 361, 388
Rodgers, S. D., & Millar, T. J. 1996, MNRAS, 280, 1046
Rozyczka, M., Bodenheimer, P., & Bell, K. R. 1994, ApJ, 423, 736
Ruffle, D. P., & Herbst, E. 2000, MNRAS, 319, 837
Ryu, D., & Goodman, J. 1982, ApJ, 338, 438
Salyk, C., Pontoppidan, K. M., Blake, G. A., Lahuis, F., van Dishoeck, E. F., & Evans, II, N. J. 2008, ApJ, 676, 49
Sandford, S. A., & Allamandola, L. J. 1990, Icarus, 87, 188
Sandford, S. A., & Allamandola, L. J. 1993, ApJ, 417, 815
Sano, T., Miyama, S. M., Umebayashi, T., & Nakano, T. 2000, ApJ, 543, 486
Semenov, D., Wiebe, D., & Henning, T. 2004, A&A, 417, 93
Semenov, D., Wiebe, D., & Henning, T. 2006, ApJ, 647, 57
Shalybkov, D., & Rüdiger, G. 2005, A&A, 438, 411
Tielens, A. G. G. M. 1983, A&A, 119, 177
Tielens, A. G. G. M., & Allamandola, L. J. 1987, in Physical Processes in Interstellar Clouds, ed. G. E. Morfill & M. Schöler (Dordrecht: Reidel), 333
Tscharnuter, W. M., & Gail, H.-P. 2007, A&A, 463, 369
Umebayashi, T., & Nakano, T. 1980, PASJ, 32, 405
Umebayashi, T., & Nakano, T. 1981, PASJ, 33, 617
Urpin, V. A. 1984, AZh, 61, 84
van Dishoeck, E. F., Thi, W.-F., & van Zadelhoff, G.-J. 2003, A&A, 400, 1
van Zadelhoff, G.-J., Aikawa, Y., Hogerheijde, M. R., & van Dishoeck, E. F. 2003, A&A, 397, 789
Verner, D. A., & Yakovlev, D. G. 1995, A&AS, 109, 125
Watson, D. M., et al. 2007, Nature, 448, 1026
Willacy, K. 2007, ApJ, 660, 441
Willacy, K., Klahr, H. H., Millar, T. J., & Henning, T. 1998, A&A, 338, 995
Willacy, K., Langer, W., Allen, M., & Bryden, G. 2006, ApJ, 644, 1202
Willacy, K., & Langer, W. D. 2000, ApJ, 544, 903
Woods, P. M., & Willacy, K. 2009, ApJ, 693, 1360
Zolensky, M. E., et al. 2006, Science, 314, 1735